HYBRID MICROFLUIDIC DEVICES FOR ON-DEMAND MANIPULATION AND SCREENING OF NEURONS AND ORGANS OF SMALL MODEL ORGANISMS

RAMTIN ARDESHIRI

A THESIS SUBMITTED TO
THE FACULTY OF GRADUATE STUDIES
IN PARTIAL FULFILLMENT OF THE REQUIREMENTS FOR THE DEGREE OF
MASTER OF APPLIED SCIENCE

GRADUATE PROGRAM IN MECHANICAL ENGINEERING
YORK UNIVERSITY
TORONTO, ONTARIO

AUGUST 2016

ABSTRACT

Caenorhabditis elegans and *Drosophila melanogaster* are widely used model organisms for neurological and cardiac studies due to their simple neuronal and cardiac systems, genome similarity to humans, and ease of maintenance in laboratories. However, their 50µm-1mm sizes and continuous mobility impede their precise spatiotemporal manipulation, thereby, reducing the throughput of biological assays. By integrating glass capillaries into microfluidic devices and using 3D-printed fixtures for precise control, we have developed hybrid lab-on-a-chip devices to facilitate the processes of animal manipulation and stimuli control, using modules for single-organism selection, orientation, imaging and chemical stimulation. These microdevices enabled us to manipulate organisms individually and to orient them at any desired direction for imaging purposes. The applications of these hybrid microdevices were demonstrated in the optical and fluorescent imaging of *C. elegans* cells as well as cardiac screening of *Drosophila* larvae. This technique can be applied in fundamental biology, toxicology, and drug discovery.

ACKNOWLEDGEMENTS

I would like to thank Dr. Rezai, for giving me the opportunity to switch from Louisiana Tech University to York University and pursue biomicrofluidics. During my M.Sc., I became a better researcher with six poster presentations, three conference papers and one journal paper. Next, I would like to thank Dr. Mei Zhen from Mount Sinai Hospital, who gave me unconditional access to her lab and instruments for my *C. elegans* research along providing essential criticism. Special thanks in this area goes to Dr. Ben Mulcahy for his very informative discussions and crucial collaboration on the *C. elegans* project. Other people who helped and thought me how to keep my stock, pick worms, perform various biological experiments were: Dr. Shangbang Gao and Dr. Maria Lim from Dr. Mei Zhen's group and Queenie Hu and Dayana D'Amora from Dr. Terrance Kubiseski's group. Also I should thank Romy Pabla and Cory Richman from Dr. Bhagwati Gupta's group for their advice on vulva imaging and giving me the related strain.

For *Drosophila* project, I was honored to get advice and strains from Dr. Arthur Hilliker along Dr. Mukai Spencer's advices. Rod Taylor and Jacob Leung helped me with strains and their maintenance which I am thankful for. Last but not least, I would like to thank undergraduate students who helped me to collect and analyze the data; Leya Hosseini and Negar Amini.

My journey and success would have been impossible without the help and understanding of Dr. Steven Jones and Dr. Tressa Murray from Louisiana Tech University,

Biomedical Engineering Department. Upon starting at York University, I was lucky to have Jacob Leung as my best friend and colleague. It was a very rewarding and energizing experience to work with him. Other people at York University that I can recall to thank are: Dr. Manu Pallapa, Dr. Chen Chen, Dr. Yanting Gao, Dr. Sonil Nanda, Romero Martin, Prateek Jindal, Zemina Meghji, Fabio Carminati, Hamed Almohammadi and Amin Shams Khorami.

In the writing of this thesis, I would like to thank the writing center at York University for their support and help to improve my level. Plus, Jacob Leung was a great help for me to gather my thoughts on my thesis along proof reading my thesis draft.

And last but not least acknowledgement goes to my dearest family and my supportive aunt and cousins. My journey started with a love story in United States, and it ended with a better and wiser person receiving M.Sc. in Mechanical Engineering. I am extremely thankful to my family for supporting me through my decisions in life. It is hard to live far apart, however, quality time would compensate the prolong separation time.

To my lovely family and friends

TABLE OF CONTENTS

LIST OF TABLES

LIST OF FIGURES

LIST OF ABBREVIATIONS

BPM	BeatPerMinute
C. elegans	*Caenorhabditis elegans*
CNS	Central Nervous System
DNA	DeoxyriboNucleic Acid
D. melanogaster	*Drosophila melanogaster*
DNC	Dorsal Nerve Cord
EF	Electric Field
GCaMP	Green Cyclic adenosine MonoPhosphate
GFP	Green Fluorescent Protein
HIF	Hypoxia-Inducible Factor
PBS	Phosphate-Buffered Saline
PDMS	PolyDiMethylSiloxane
RFP	Read Fluorescent Protein
S.E.M.	Standard Error of Mean
sGC	soluble Guanylyl Cyclase
VNC	Ventral Nerve Cord

Chapter 1
Introduction

Model organisms such as monkey, mouse, chicken, frog, zebrafish, *Drosophila*, *C. elegans* and yeast are widely used for genetic investigations [1], drug screening [2], and behavioural studies [3]. These model organisms can be divided into two main subgroups, i.e., vertebrates and invertebrates. While vertebrates are more similar to humans in terms of their genetics, organs, and biological functionalities, there are many challenges, such as ethical regulations and physiological complexities, involved in performing biological experiments on them [4,5]. Invertebrates on the other hand are low-cost, easy to culture and maintain in laboratories, physiologically and genetically simpler than vertebrates- yet they are relatively similar to humans, not restricted by ethical regulations, and optically accessible down to cellular level due to their almost transparent bodies. These features make invertebrates popular and widely used in a variety of fundamental and applied biological research. *Caenorhabditis elegans* and *Drosophila melanogaster* are two of the most widely used invertebrate model organisms for human diseases [6–8]. These organisms are highly homologous to humans in their genomes, which have been fully sequenced [9,10] and possess simple and structurally-known cellular and nervous systems. Moreover, a wide variety of their mutants have been made available by genetic manipulation for biological investigation of human diseases and disorders [11,12].

1.1 *C. elegans* and *D. melanogaster* as Invertebrate Model Organisms

Among the most important advantages of *C. elegans* and *D. melanogaster* are their genetic homology to humans and amenability to genetic manipulation. This makes them ideal models to investigate how genes function and encode for proteins especially in genetic disorder and disease studies. The wild type species of these organisms are widely found in nature, while a vast number of genetically-altered mutants can be naturally or experimentally created [13]. In other word, mutant strains are versions of the wild type animals carrying known defects (e.g., deletion or change) in their genome that lead to specific and desired cellular malfunctions that can be studied using a variety of screening methods. Mutation can happen when animals are exposed to certain chemicals, heat or oxygen level for generations in the nature. Moreover, a straight-forward approach to experimentally produce specific mutants is to inject desired DNAs into these organisms to produce deficiencies and defects in cells, neurons, tissues, and organs of interest. *C. elegans* and *D. melanogaster* model organisms benefit from availability of a diverse range of mutants maintained at central mutant banks that are available to the scientific community; hence, making them ideal for a wide variety of biology investigations.

Young adult *C. elegans* (Fig. 1a) is approximately 1 mm long and 40-50 µm wide with a transparent body. The life cycle of *C. elegans* is only 3 days at 25˚C and can produce around 300 progenies after reaching adulthood through self-fertilization [11]. *C. elegans* was the first model organism with a fully mapped genome that was yielded to be 60–80% homologous to humans [9]. Nonetheless, it is also a biologically simple (959 cells) model

organism which plays an important role in neuroscience research due to its simple and well-mapped neuronal system (302 neurons) and the availability of a variety of mutants [11]. *C. elegans* have been used to investigate fundamental biological processes such as apoptosis, cell signalling, cell cycle, cell polarity, gene regulation, metabolism, ageing and sex [14]. They have also been used as models for various human diseases such as studying the toxin-induced degeneration of brain dopamine neurons in Parkinson's disease [15,16].

Early-stage 3rd instar *Drosophila* larva (Fig. 1b) is approximately 3.5 mm long and 0.7 mm wide and has a semi-transparent body. The animal's full life cycle is 10 days at 25˚C, and adult flies can produce hundreds of genetically identical offspring within 10 to 12 days [12]. Approximately 75% of specific disease genes (~14,000) are estimated to be similar between *Drosophila* and humans [12]. *Drosophila* model organism benefits from a fully sequenced genome with a rich bank of mutant strains available for disease studies [17]. The brain of adult fly consists of more than 100,000 neurons capable of controlling complex behaviours such as sleep, learning, courtship, feeding, aggression, grooming and flight navigation [12]. These advantages have led to emergence of *Drosophila* as one of the simplest model organisms for investigation of olfactory coding [18–20], neuropsychiatric disorders [8,21,22], pain [5,23], sleep disorders [24], chemical toxicity [25], and cardiac diseases [26–29] such as congenital heart disease and cardiomyopathies [30].

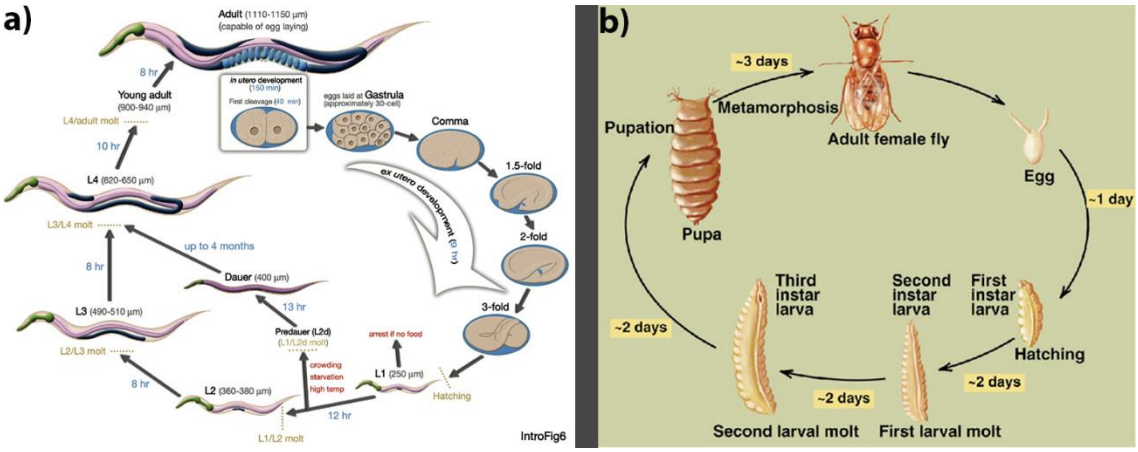

Figure 1: Life cycle of a) C. elegans [31] *and b) D. melanogaster* [32].

Manipulation of these small-scale organisms, including their delivery, orientation, and immobilization, plays a critical role in the biological assays that have employed such organisms to answer fundamental questions about human disease causes, pathways and treatments. For instance, *C. elegans* vulva muscles and neurons are located in ventral side of the worm, and ventral orientation is needed to better observe them [33]**.** *Drosophila* larval cardiac tubes are located at the dorsal vessel, and proper dorsal orientation with full immobilization is required for monitoring the heart activities in intact animals, which otherwise will not be visible due to their semi-transparent cuticle [34]. The importance of precise manipulation of these model organisms in desired longitudinal and lateral (dorsal-ventral, left-right, or in between) orientations cannot be overstated. Such manipulation is crucial for accessing target cells, neurons and organs of interest in various studies such as cellular and neural imaging [35,36], cell ablation [33,37], microinjection [38] and electrophysiology [39].

1.2 Conventional Manipulation Methods to Orient and Immobilize Small Model Organisms

There is a need in different studies for manipulation of *C. elegans* and *D. melanogaster* individually or in groups. For individual animal-based studies, tweezers and worm picks were used to orient the animal in proper directions. Then, double-sided tape or glue was conventionally used to permanently immobilize them onto the substrate for post-immobilization assays. For group-based assays, a population of animals were distributed on a surface and immobilized mechanically with a glass slide being placed on top of them. Orientation was random via this method; however, some animals with the desired orientation could be selected and studied. For instance, Zhang et al. oriented single worms in dorso-ventral direction to observe VC4/5 and HSN neurons (VC: Ventral Cord, HSN: Hermaphrodite Specific Neuron) simultaneously to investigate the role of these motor neurons in egg laying [35]. Different mutants (i.e., HSN^-, VC^-, $VC4/5^-$) and their neuronal responses to serotonin, acetylcholine (ACh) and gentle touch were investigated to elucidate the importance of HSN neurons in reproduction and show their activation during egg laying [35]. Moreover, interfering with ACh neurotransmission was shown to block the egg laying process (same as gentle touch), while serotonin excited the neurons and increased egg laying. Badre et al. oriented semi-dissected *Drosophila* larva and exposed the larva's heart to air, CO_2 and N_2 [40]. Complete stoppage of the heart and body wall movements was observed in case of CO_2, while N_2 exposure decreased these functions during the 10 minutes exposure.

The above-mentioned manual methods to manipulate individual organisms require a high level of expertise and can be harmful to delicate animals if not executed with care. Besides requiring expertise, they are also time-consuming, labour-intensive, and low in throughput. The batch-based method is not as laborious, but it requires a large sample population while returning a low yield in properly oriented animals. These animals are usually not accessible for post-orientation procedures such as chemical exposure and screening. Moreover, the glue-based immobilization method is irreversible and not useful for post-exposure assays, in which animals should recover and be preserved for long-term investigations.

1.3 Microfluidic Methods to Orient and Immobilize Small Model Organisms

In the past decade, many microfluidic devices have been developed to facilitate automation and enhance the throughput of experiments on small model organisms, such as *C. elegans*, *D. melanogaster*, and *D. rerio* [41–43]. For instance, microfluidic devices have been developed for automated manipulation and sorting [44–46], imaging and monitoring [47,48], behavioral screening [49–51], extracellular electrophysiological signal recording [52,53] and microinjection [54,55] of *C. elegans*. Regarding *Drosophila* larva, a smaller variety of microfluidic devices have been developed for the primary application of imaging and monitoring neuronal activities [37,56,57]. The amount of literature in this area is very extensive and the readers are referred to thorough review papers by Wlodkowic et al. [41], Yanik et al. [58], Crane et al.[59], and Gupta and Rezai [43] to gain a comprehensive

understanding of application of microfluidics in small-organism studies. Here, we focus our review on the application of microfluidic devices for animal manipulation, which mainly consists of orientation and immobilization of organisms in the devices.

1.3.1 Orientation of Small Model Organisms

Orientation of small organisms has been achieved with passive and active methods. *C. elegans* passive orientation (Fig. 2a) was achieved by Cáceres et al. [60] as they developed a U-shaped microfluidic channel (radius of curvature=125μm) to laterally orient *C. elegans* with 84% efficiency in the dorsal-ventral direction. The curvature of the channel mimicked the crawling environment of the worm and hence it oriented the animal laterally as it was passed inside the channel with hydrodynamic pressure. The orientation enabled successful monitoring and sorting of different mutants based on their commissural neuron appearances. However, animals could only be oriented dorsally or ventrally and the position of worms' ventral or dorsal side after orientation was completely random with 59% of worms' ventral side facing the inside of the U-channel. This device could not achieve any other desirable orientation directions that may be needed in different assays.

In active methods, an external power source is used to rotate the organism to a desired angle. For instance, cells [61], *C. elegans* [62] and zebrafish larvae [63,64] have been successfully oriented inside glass capillaries that could be rotated by external actuators. Rieckher et al. [62] used a pulled borosilicate glass capillary that was connected to a stepper motor for worm rotation. Worms were immobilized for 15 minutes in 10 mM levamisole or sodium azide prior to imaging. Immobilized adult worms were loaded into

the glass capillary filled with 87% glycerol solution to minimize light reflective index and to achieve higher quality images with an approximate resolution of 2μm. Another recent active method used acoustic waves to rotate small organisms in a microchannel. This acoustofluidic rotational manipulation (ARM) technique (Fig. 2b) was developed by Ahmed et al. [65] to investigate defective vulval morphologies in *C. elegans* mutants by continuously rotating and imaging anesthetized worms in a microchannel. Micro-vortices generated by acoustically-oscillating microbubbles have been used for this purpose. 3D images of *C. elegans* were constructed by combining 2D images of the worm taken during a 360 degree rotation. The use of anesthetized worms is not highly desired for long-term biological investigations. Additionally, complete pressure equilibrium, proper transducer alignment on the chip and trapped air bubbles in the microchannel were critical for achieving controllable orientation, which can impede further integration of this technique. Surprisingly, no microfluidic devices for orientation of *Drosophila* larva has been reported to date.

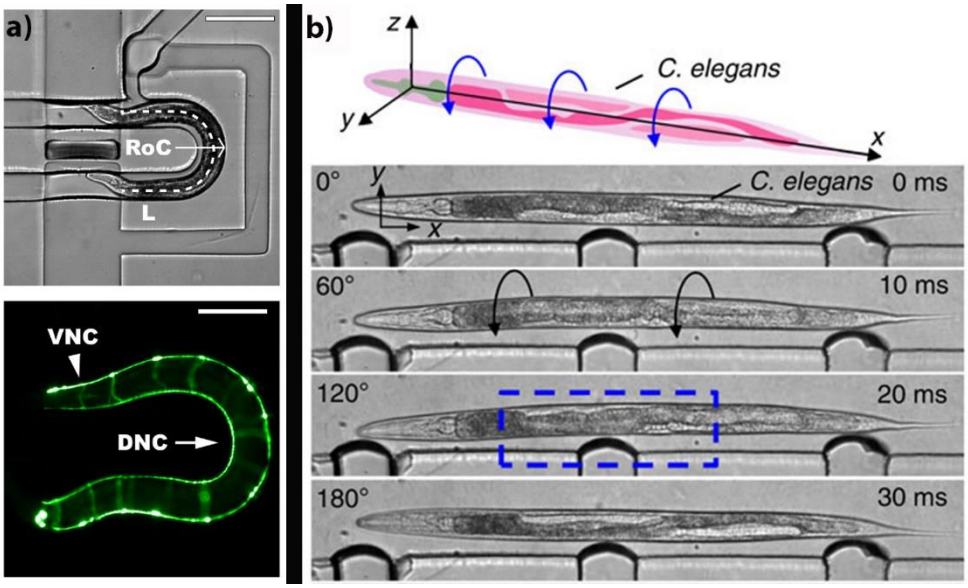

Figure 2: Microfluidic devices used for C. elegans orientation using a) U-shaped passive microchannel for dorso-ventral orientation [60] *and b) acoustofluidic rotational manipulation (ARM) for multidirectional orientation* [65].

There is a need for development of a simple microfluidic device that can aid orienting unanesthetized organisms at any desired angle with post-orientation access to the specimen for various purposes such as chemical exposure and neuron or organ level response investigations.

1.3.2 Immobilization of Small Model Organisms

Previously developed microfluidic devices for *C. elegans* and *D. melanogaster* immobilization can be categorized into five major groups based on their immobilization technique using tapered channels [57,66], side suction channels [45], deflectable membranes [37,67] and external stimuli such as cooling [68] or CO_2 exposure [37,67].

Furthermore, these methods can be combined (e.g., deflectable membrane with cooling) to increase the efficiency of immobilization.

Tapered Channel Technique

The devices in this method contain tapered microchannels to mechanically constrain the animals within the narrow channel as they are loaded into the device hydrodynamically. This method is easy to use and has been utilized for immobilization of both *C. elegans* [66] and *Drosophila* [57]. By parallelizing the tapered channels, Hulme et al. [66] (Fig. 3a) were able to immobilize 116 adult worms successfully inside a 128-clamp microdevice within 15 minutes for imaging purposes. Worms were then released and no significant damage to their internal anatomical structure, behaviour, survival, and progeny-production was observed. Ghaemi et al. [57] applied this technique to immobilize 3rd instar *Drosophila* larva for GCaMP calcium indicator monitoring of Central Nervous System (CNS) activities, as shown in Fig. 3b. CNS responses to different sound frequencies (50-5000 Hz) and intensities (95-115 dB) were investigated. It was found that increase of frequency from 50 to 200 Hz increased the CNS activity; however, further frequency increase to 5 KHz resulted in decrease of CNS activities in the immobilized larvae. At any particular frequency, CNS activity had direct correlation with the signal intensity (dB), meaning stronger audio signals led to higher CNS fluorescent responses.

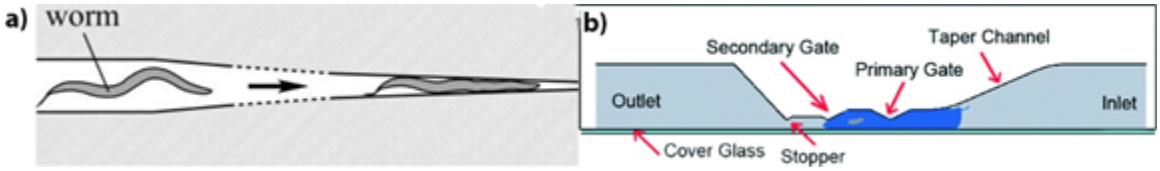

Figure 3: Use of tapered channels for immobilization of a) C. elegans [66] *and b) Drosophila larva* [57]. *Reproduced with permission from Royal Society of Chemistry.*

This technique is amenable to parallelization and will provide robust and desirable immobilization that can simply be integrated into any high throughput chip design. However, downsides of this simple technique are the lack of access to the body of organisms for chemical exposure, associated risk of ejecting the animals via fluid flow, and the possibility of applying excess forces onto animals' cuticle if pressure is not properly regulated.

Side Suction Technique

In this technique, organisms are captured pneumatically in a channel by the aid of small side suction channels. Rohde et al. [45] used side suction immobilization to select, image and sort *C. elegans* worms as shown in Fig. 4. The device consisted of multiple microvalves to operate different channels in the devices such as loading, waste, wash, suction, and collection channels as shown in Fig 4a. Single side suction was used to capture one worm form a population while the rest of the worms were washed into the waste channel. The selected worm was then immobilized by the array of side suction channels and microsurgery of neural axon was performed by laser ablation. Song et al. [55] utilized this technique for high speed microinjection of *C. elegans.* To date, this immobilization

technique has not been applied to *Drosophila* larva. Advantages of this immobilization method are control over pressure intensity in the suction channels to reduce excessive forces exerted on the immobilized animal and accessibility of the specimen for post-immobilization studies such as chemical exposure and organ-level monitoring. However, this immobilization method is not as robust as CO_2 exposure or deflectable membrane techniques (see next sections) and the animal can still flex its body at the side that is not immobilized by suction forces.

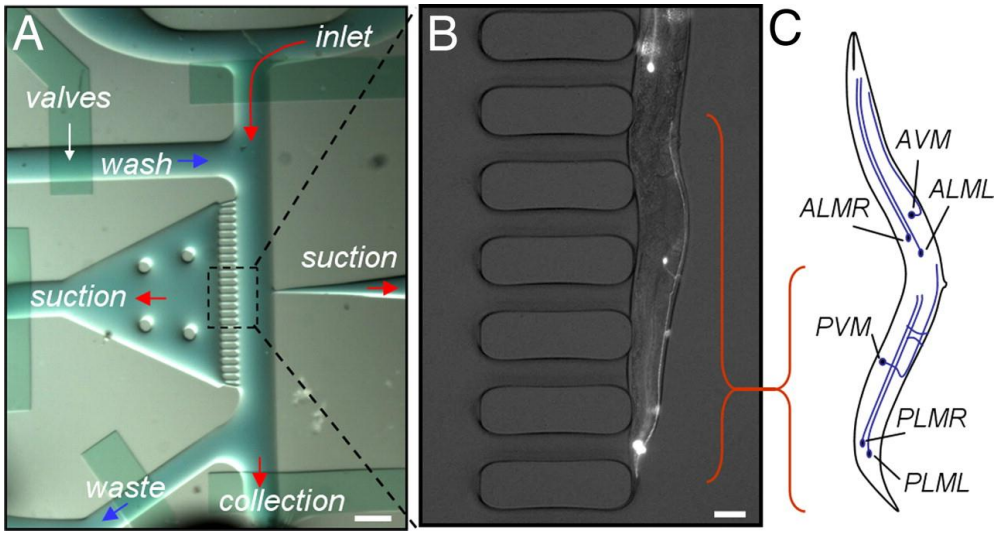

Figure 4: Side suction technique to immobilize C. elegans adult worm [45]. *Reproduced with permission from National Academy of Sciences, U.S.A.*

PDMS Deflectable Membrane Technique

In this technique, organisms are positioned in a section of the device with a deflectable polymeric membrane above their bodies. Pressurizing the membrane from the top leads to its deflection onto the organism's body and immobilization in the device

(Fig.5). *C. elegans* [67] and 3rd instar *Drosophila* larva [37] have both been immobilized with this technique for imaging and monitoring of neurons and body organs. Survival rate for *Drosophila* larva was reported to be more than 90% after one-hour immobilization with a deflectable membrane [37]. Mondal et al. [69] used this technique to immobilize different model organisms at different pressures, i.e., *C. elegans* at 14 psi, *Drosophila* at 7 psi and zebrafish at 3 psi. Membrane thickness for *C. elegans* was 80 µm, whereas a thicker 300 µm membrane was needed for immobilizing *Drosophila* and zebrafish.

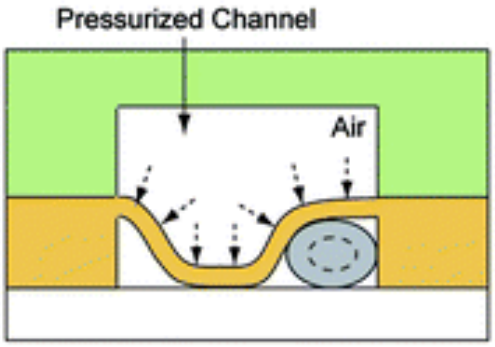

Figure 5: Deflectable membrane immobilization of C. elegans in a microchannel [67]. *Increase in air pressure at the top channel leads to deformation of the thin membrane and confinement of the worm in the bottom channel. Reproduced with permission from Royal Society of Chemistry.*

Deflectable membrane technique provides better immobilization compared to tapered channel and side suction techniques. However, it results in animal body deformation, which makes it not suitable for applications where organ morphology and function (e.g., *C. elegans'* vulva or *Drosophila's* heart functions) should be investigated. Moreover, this technique is not compatible with liquid exposure modules for chemical screening since there cannot be a flow in the channel while the membrane is deflected. Gas

exposure is achievable due to permeability of gases trough the pores of the membrane which is usually polydimethylsiloxane (PDMS).

CO_2 Exposure Technique

CO_2 as an aesthetic gas has been used for immobilization of both *C. elegans* [67] and *Drosophila* [37]. Chokshi et al. [67] showed *C. elegans* immobilization by 100% CO_2 infusion through a 30µm thick PDMS membrane at the pressure of 10 psi (Fig. 6a). Worms were fully immobilized within 1-2 minutes of exposure and were successfully recovered after 2.5 hours post-exposure. However, CO_2 was shown to inhibit neuromuscular junction (NMJ) transmission and be lethal after 3 hours of direct exposure. Ghannad-Rezaie et al. [37] exposed 3rd instar *Drosophila* larva to CO_2/air (95/5%) mixture through a 10 µm thick PDMS membrane at 5 psi pressure (Fig. 6b). CO_2/air exposure was applied for only 30 seconds during 5-minute immobilization intervals to minimize the toxic effects of CO_2. With this immobilization technique, neuronal responses before and after laser injury were monitored, and the recovery of injured neurons was quantitatively reported using fluorescent microscopy.

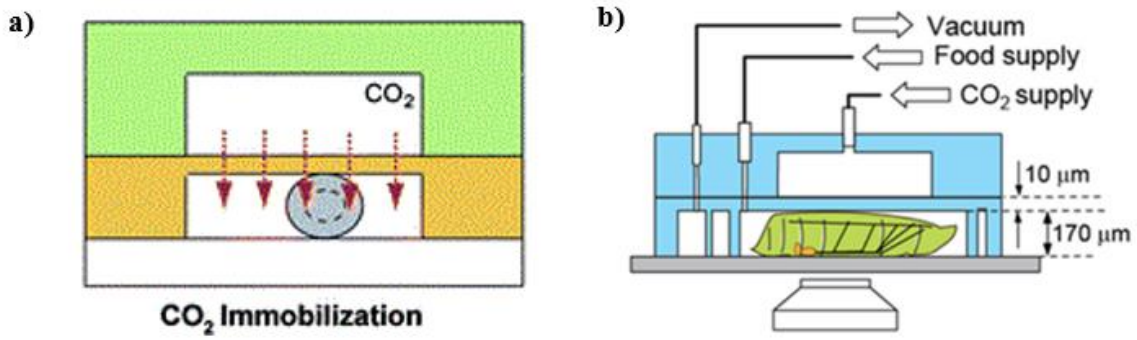

Figure 6: CO_2 exposure for immobilization of a) C. elegans [67] *and b) Drosophila larva* [37]. *Reproduced with permission from Royal Society of Chemistry.*

CO_2 can be beneficial for short-term immobilization due to its quick effect, fast recovery, and minimized mechanical stress on animals. However, this method should be avoided when physiological states of neurons and organs (e.g., *Drosophila's* heart activities) are the subject of investigation in different assays.

1.4 Research Goals and Objectives

Our goal in this research was to develop a microfluidic technique for on-demand and reversible orientation and immobilization of small model organisms (*C. elegans* and *D. melanogaster*) for imaging of their neurons and organs (e.g., vulva and heart). The organisms were required to be accessible during immobilization for chemical screening assays. To achieve our goal, the set of objectives listed below were pursued in designing a microfluidic device.

1) Select a single organism from a population with desired longitudinal orientation (i.e., head loading).

2) Pneumatically capture the selected organism with a glass capillary while minimizing the damage on its body and behavior.

3) Control the rotation of glass capillary for lateral orientation of captured organisms.

4) Investigate whether organisms can be released after orientation and immobilized conserving their orientation.

5) Screen organisms during immobilization to demonstrate the application of our technique in neuronal imaging and cardiac chemical assays.

1.5 Thesis Structure

This research is centered around the idea of implementing rotatable glass capillaries inside microfluidic devices in order to address the challenges associated with multi-directional orientation and screening of small scale model organisms as discussed in this chapter. In chapter 2, we will describe the methodologies and materials used in our research to develop and characterize the aforementioned hybrid microfluidic devices. In chapter 3, the application of these microfluidic devices in *C. elegans* multidirectional orientation and fluorescent imaging of neurons will be presented. However, the idea of using a rotatable glass capillary in a microdevice is not restricted to *C. elegans*. In Chapter 4, we will demonstrate the application of a hybrid microfluidic device, similar in working principles to the one used in Chapter 3, in manipulating *D. melanogaster* larvae on a chip. In this chapter, we will add a chemical exposure module to our device and demonstrate its

capability in screening cardiac activities of intact *Drosophila*, which was made possible after proper orientation of the larva in our chip. A summary of the work and possible future directions are presented in chapter 5.

Chapter 2
Materials and Method

2.1 Organism Preparation

Wild type N2 strain worms were used in bright field imaging experiments. DY576: *him-8 (e1489)*; *nIs96*[*Plin-11*::GFP)]) and SGP14: *sgpIs7*[F25B3.3::TagRFP,pJM24] strains were obtained from Dr. Bhagwati Gupta (McMaster University) and Dr. Mei Zhen (University of Toronto) labs respectively, and used for fluorescent imaging of uv1 and vulB1\2 cells as well as the ventral nerve cord (VNC). All experiments were performed using synchronized young adult worms at ambient temperature (approximately 22 ºC). Gravid worms were initially washed from the Nematode Growth Medium (NGM) plate with M9 buffer (3g KH_2PO_4, 6 g Na_2HPO_4, 5 g NaCl, and 1 mL 1M $MgSO_4$ in 1L) and centrifuged for 1 min at 1200 rpm (revolutions per minute). Excessive liquid was removed, leaving behind the worm pellet. Worms were bleached (8.25 mL ddH_2O, 3.75 mL 1M NaOH, 3.0 mL bleach) and hand shaken for 5 minutes and centrifuged for 1 minute at 5000 rpm. Collected eggs were then washed three times with M9 for 1 min at 5000 rpm. Embryos were hatched and halted at the L1-L2 stage after 24 hours post bleaching. The worms were then transferred onto a new NGM plate, and the growth was monitored until the L4 stage. Experiments took place 24 hours post L4 stage on young adult animals. Prior to each experiment, worms were washed with M9 from the plate, centrifuged (1200 rpm) and washed three times to clean the sample.

White (w^1) *Drosophila melanogaster* larvae were mass cultured on standard yeast media in fly stock bottles at ambient temperature (approximately 22 ºC). Prior to the experiments, adult flies were emptied from the bottle, and wandering 3rd instar larvae were transferred from the bottle to a Phosphate-Buffered Saline (PBS) solution using a spatula.

2.2 Chemicals and Reagents

Cyanoacrylates glue (LePage Ultra Gel, PN#1471916) was used for conventional immobilization of *Drosophila* larvae (as a control experiment) where immobilization in the microfluidic chip was being investigated. For chemical screening studies, sodium azide (NaN_3) purchased from Sigma Aldrich, Canada, and oxygen (O_2), nitrogen (N_2), compressed air, and carbon dioxide (CO_2) gas cylinders purchased from Linde (Canada) were used. Table 1 shows the concentration level of these chemicals used in our assays for screening the effect of sodium azide, oxygen, and carbon dioxide on cardiac activities of intact *Drosophila melanogaster* larvae. Sodium azide solutions were prepared off the chip

Table 1: Aqueous and gaseous chemical screening assays and their chemical constituents and concentrations

Chemical Screening Assay	Concentration Level (%)	Chemical Composition					
		NaN3 (g)	DI Water (g)	O2 (mL/min)	N2 (mL/min)	Air (mL/min)	CO2 (mL/min)
Sodium azide*	20	20	80				
	10	10	90				
Oxygen	100			50			
	21					50	
	0				50		
Carbon dioxide	100						50
	50					25	25

* Chemicals mixed in the ratios above and introduced at 1 mL/min into the device

at 10% and 20% concentration levels. Carbon dioxide at 50% concentration (with air as the balancing gas) was generated using two flow regulators (25 ml/min each) attached to the carbon dioxide and air cylinders.

2.3 Microfluidic Device Fabrication by Soft Lithography

To fabricate microfluidic devices with soft lithography, a 2D design of the chip was sketched in AutoCAD (Autodesk Inc., USA). The sketched design was printed with a µPG501 chromium mask writer (Heidelberg GmbH, Germany) on a glass mask. Photoresist (SU8-2035 MircoChem, USA) was spun at 1400 rpm on a 3" silicon wafer, resulting in a 65 µm thickness. After soft baking (65˚C for 2 min and 95˚C for 8 min), the wafer was placed in a EVG 620 mask aligner (EV Group Inc., USA) with the printed mask on top, and was exposed to the UV light (250 mJ/cm^2) in order to crosslink desired features on the wafer. Post-exposure bake (65˚C for 2 min and 95˚C for 7 min) was performed after UV exposure. The baked wafer was then developed with SU-8 developer for approximately 7 min until the desired features were observed, rinsed with SU-8 developer and isopropyl alcohol (IPA), and dried with N_2 gun to obtain the master mold. Feature sizes were measured with Bruker optical profiler (Bruker Optics, USA). PDMS was used to produce a negative replica of the master mold. A 1 mm-diameter glass capillary was then fixed with half-cured PDMS on the master mold (at desired location) in order to serve as the housing for later-stage installation of the rotatable glass capillary. Subsequently, PDMS (10:1 ratio of elastomer and curing agent, SYLGARD 184, Dow Corning, USA) was poured over the master mold, and cured for 3 hr at 80˚C. After peeling off the cured PDMS

layer, the glass capillary was removed, and the rotatable glass capillary was pre-loaded into its location. This layer was then oxygen plasma bonded at 900 mTorr pressure and 50 W power for 30 seconds (PDC-001-HP Harrick Plasma, USA) to another flat PDMS layer.

2.4 Microfluidic Device Fabrication with 3D-printing

These microfluidic devices consisted of two PDMS layers. The top layer was fabricated by replica molding of PDMS (10:1 ratio) onto a 3D-printed (ProJet HD 3000, 3D Systems, USA) plastic master mold and contained the network of desired microchannels. PDMS pre-polymer was poured over the master mold and cured at 80ºC for 3 hours. The bottom PDMS layer was fabricated by casting the same mixture of PDMS onto a petri dish and curing at 80ºC for 3 hours. The two PDMS layers and a glass slide (35 mm × 50 mm glass slide (Fisher Scientific)) for back-support were bonded to each other by oxygen plasma bonding at 1 Torr pressure and 50 W power for 90 seconds (PDC-001-HP Harrick Plasma, USA). Glass capillaries were then installed into specific inlets and connected to syringes for loading of organisms or applying a negative pressure for capturing and orientation.

2.5 Glass Capillary Fabrication

The glass capillaries for *C. elegans* orientation (1B100-4, World Precision Instruments Inc., USA) were pulled by Sutter P-1000 (Sutter Instrument, USA) with the Bee-Stinger recipe [70] and were broken at the tip to provide 30 µm inner diameter (ID). A 1.1 mm inner diameter glass capillary (Fisher Scientific, P# 22-260-943) was used as a loading

capillary for *Drosophila* larvae and a 0.4 mm inner diameter glass capillary (Fisher Scientific, P# 1-000-0040) was used for orientation.

2.6 Image and Video Recording and Analysis

All devices were tested under an inverted microscope (BIM-500FLD, Bioimager Inc., Canada) equipped with a camera (GS3-U3-23S6M-C, Point Grey Research Inc., Canada) for capturing bright-field and florescent images as well as videos on a computer. These images and videos were analyzed using the ImageJ software.

2.7 Chemotaxis Assay

To investigate the effect of manipulating organisms with the glass capillary, a chemotaxis assay (4 trials in triplicate, N≈20 worms per experiment) was performed off the chip to avoid the possibility of mixing treated worms with the untreated ones. A 200 µL suspension of worms was pipetted onto a petri dish and placed under the microscope adjacent to the tip of a glass capillary connected to the regulated vacuum source. Worms were captured individually in a way that not more than 30% of their bodies were drawn into the glass capillary in one minute (as practiced in the chip). After one minute, pressure was turned off, and worms were released into a M9 droplet. The captured worms were then transferred to a food race plate and placed 5 cm away from a 0.5 mm-diameter Escherichia coli (OP50) colony. Worms' movement towards the food colony was monitored for two hours. Every 10 minutes, worms that reached the food colony were counted and discarded. At the end of two hours, the remaining worms were counted to obtain the total number of

worms. Same chemotaxis experiment was performed for parallel control groups which went through the same procedure without the glass capillary manipulation.

2.8 Statistical Analysis

GraphPad Prism software (version 6.07, GraphPad Software Inc., USA) was used for statistical analysis and conclusions were made based on the p-values. In all cases except chemotaxis experiment, two-tail unpaired t-test was used to show the significant difference (p-values and confidence levels) between two different groups of investigated organisms. For the chemotaxis experiment, two-way ANOVA test was used to investigate the effects of two variables (manipulation condition and time) on chemotaxis behaviour. The effect size (Cohen's d-value for t-test and r-value for ANOVA) and statistical power (1-β) were calculated in our experiments [71], to provide more information about the size and confidence of investigated effects. Finally, if $p<0.05$, data was deemed statistically significant with the calculated effect size of $d<0.2$ as small effect, $d<0.5$ as medium effect and $d>0.8$ as large effect [72].

Chapter 3
Longitudinal and Lateral Orientation of *C. elegans* and Multidirectional Imaging of Neurons and Organs

3.1 Design and Fabrication of the Hybrid Microfluidic Device

The microfluidic chip (Fig. 7a) was fabricated using the soft lithography method discussed in Chapter 2 and consisted of three major components, i.e., a single worm selection module, an orientation and imaging channel, and a rotatable glass capillary actuator shown in Fig. 7b at 5x magnification. The worm selection module was designed to enable loading of one worm at a time into the imaging channel. This module contained positive and negative electrodes inserted into the reservoirs of input and recirculation channels as well as a tapered microchannel (narrowing from 35 μm to 25 μm width) to trap a young adult worm from a synchronized population. The orientation and imaging channel included a 65 μm wide microchannel for lateral manipulation with side suction channels to immobilize the worm (480 μm total length). The rotatable glass capillary actuator was placed in front of the orientation and imaging channel and was used to capture the head of the worm and rotate it until reaching the desired orientation.

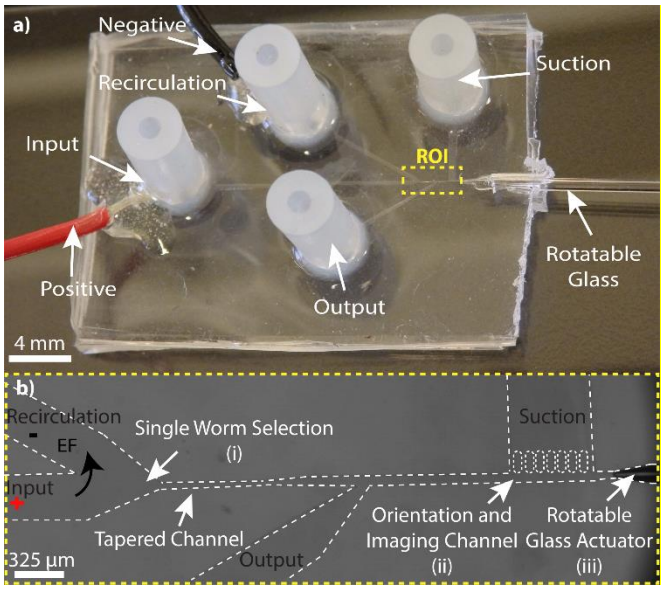

Figure 7: (a) An overview of the hybrid microfluidic chip for C. elegans longitudinal and lateral orientation and imaging. (b) Region of Interest (ROI) of the microfluidic chip and its modules, i.e.,: (i) single worm selection, (ii) orientation and imaging channel, and (iii) rotatable glass capillary actuator. Channel height was 65µm.

3.2 Experimental Setup for *C. elegans* Longitudinal and Lateral Orientation

The described hybrid microfluidic device (Fig. 7) was used to select and load a single worm from a synchronized young adult worm population, then rotate and orient it at desired angles via rotating the glass capillary, and finally image it optically or fluorescently inside the device. Fig. 8a shows the overall experimental setup used for on-demand orientation of *C. elegans*, which was necessary for the operation of the microfluidic device. The setup consisted of three main modules, i.e., a 3D-printed fixture to operate the hybrid microfluidic device, a sample manipulation module to control worms' orientation in the device, and image acquisition and analysis components.

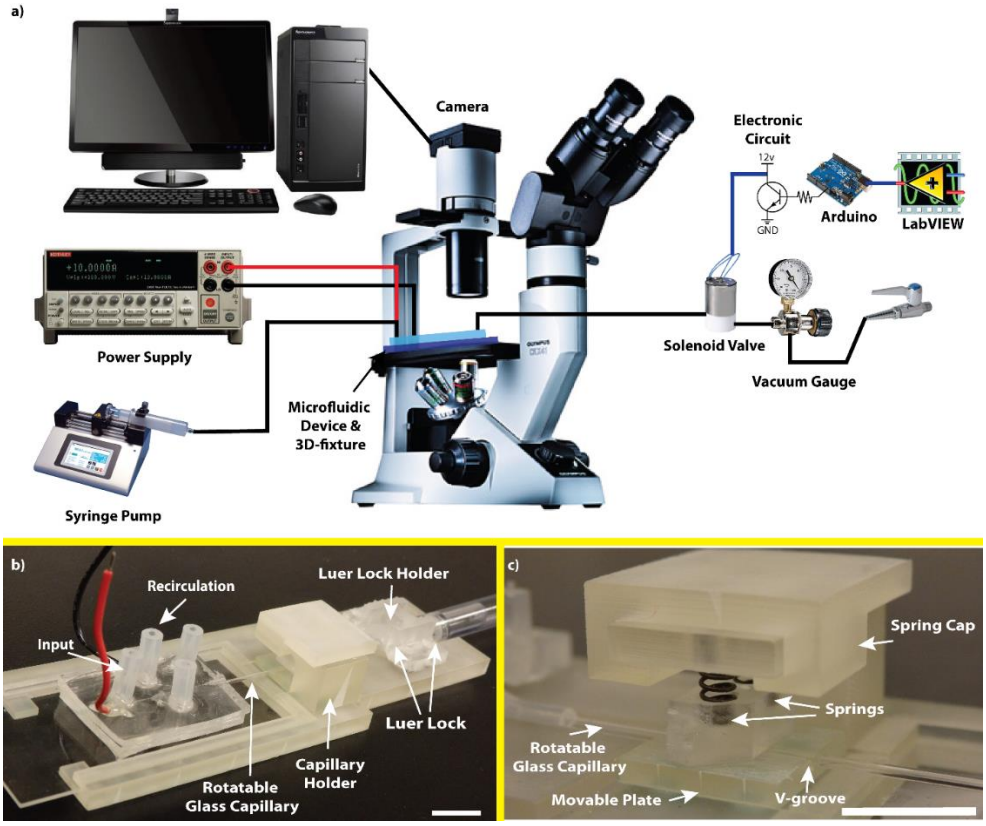

Figure 8: (a) Experimental setup consisting of microscope, hybrid microfluidic device, 3D-printed fixture, DC power supply, solenoid valve, syringe pump, vacuum gauge and electronic components. (b) 3D-printed fixture included a luer-lock holder, a glass capillary holder, and a space for positioning the microfluidic chip. (c) Glass capillary holder showing a movable plate containing a v-groove, the rotatable glass capillary, two springs and a spring cap. Scale bar: 1cm

One of the most important functions of the microfluidic chip was its ability to provide accurate rotation of the glass capillary inside the imaging channel to facilitate precise *C. elegans* orientation on the chip. For this, a fixture shown in Fig. 8b was designed and 3D-printed with a ProJet HD 3000 printer (3D Systems, USA). The 3D-printed fixture included a luer-lock holder, a glass capillary holder, and a space for positioning the microfluidic chip. The glass capillary holder (Fig. 8c) consisted of a movable v-groove

plate, a spring housing to hold two springs, and a spring cap to secure the glass capillary by the springs. The microfluidic device was inserted into the 3D-printed fixture, and the glass capillary was secured in the v-groove plate via the glass capillary holder to minimize its lateral and vertical movements. The glass capillary was then connected to a 1 mL syringe via a 0.8 mm silicone tube and two luer-lock connectors. This syringe was used to apply manual rotation to the glass capillary and hence to the worm. The luer-lock holder was used to secure the connectors attached to the syringe in place to prevent any axial movement artifacts to be delivered to the glass capillary in the device.

The sample manipulation module consisted of a syringe pump, a DC power supply, and a regulated lab-bench vacuum source controlled by a solenoid valve system. The syringe pump (Legato 110, KD Scientific Inc., USA) was used to deliver a population of synchronized worms into the input channel. The DC power supply (KEITHLEY 2636, Keithley Instruments Inc., USA) was used to apply a desired DC electric field for longitudinal orientation of the worms [49,73]. The lab-bench vacuum source was regulated by a vacuum gauge (0-15 psi, Cole-Palmer, USA) and pulsed to the glass capillary actuator in the device by a solenoid valve (3-Way direct lift solenoid valve (12 volts), Cole-Palmer, USA). The operation of the solenoid valve was controlled by a microprocessor (Arduino Uno, Arduino LLC, Italy) and a simple electronic circuit (resistors and a NPN transistor) to provide 12 volts pulsations. LabVIEW (National Instruments, USA) was used to control the microprocessor and to apply different waveform frequencies. Pulsed and regulated

suction was applied through a 1/16th silicon tube which was press-fitted to the end of the 1 mL syringe connected to the glass capillary.

3.3 Experimental Procedure to Operate *C. elegans* Hybrid Microfluidic Device

A synchronized population of young adult worms was delivered to the middle of the input channel using the syringe pump. The flow was stabilized and a 2.6 V/cm electrical field [49] (desired for young adults) was applied to the worms to instigate their longitudinal orientation towards the tapered worm selector channel. The worms were then pushed towards the worm selector with various flow rates and possibility of trapping a single worm in the tapered channel while washing the rest of them out through the recirculation channel was investigated. After this step, the recirculation channel was closed in order to load the selected worm into the orientation and imaging channel. The effects of vacuum pressure magnitude and pulsation frequency on capturing the worm with the rotatable glass capillary were investigated for later-stage lateral manipulation and imaging. Images of manipulated worms were taken at 10x magnification for further dimensional analysis by ImageJ software. The percentage of worm body left outside of the glass capillary (inside the imaging channel) was used to determine the best setting for pneumatic manipulation of worms. The selected setting was then used for lateral manipulation of three different strains of *C. elegans* in the chip and their multidirectional imaging. To demonstrate different orientations, bright field and fluorescent images (red and green) of different organs and neurons were obtained. The vulva in wild type worms is easily recognizable, lies on the

ventral side of the worm, and can be used to determine different orientations in bright field images. VNC neurons were imaged in pan-neuronal RFP strain (SGP14) at different orientations. VNC was used for orientation demonstration as it contained 80% of neurons in comparison to 20% for dorsal nerve cord (DNC), hence was seen as a single bright nerve cord along the ventral side of the worm. Further, the developed device enabled us to observe vulva cells (uv1 and vulB1\2) at three distinct orientations under 10x magnification in DY576 strain.

3.4 Results and Discussions

The novel hybrid microfluidic device shown in Fig. 7 was developed to address the technological need in *C. elegans* studies requiring desired longitudinal and lateral orientation. It enables on-demand orientation and multi-directional imaging of organs and neurons with no need for anesthetizing the animals while providing post-orientation access to the worm. Operation of the device was facilitated by a custom-designed 3D-printed fixture and an experimental setup shown in Fig. 8.

3.4.1 Precise Rotation of Glass Capillary in the Hybrid Microfluidic Chip

Successful orientation of a worm inside our microfluidic chip depended strongly on smooth and precise rotation of the glass capillary inside the orientation and imaging channel. We determined that axial, lateral and vertical displacements of the glass capillary tip during a full rotation should not have exceeded 30 μm inside the chip. This range was

selected to prevent the glass capillary tip (OD≈40 μm) from contacting the channel walls that could result either in its breakage or blockage by residual PDMS. In order to achieve precision in the glass capillary rotation and minimize its movements in the device, we designed and developed a 3D-printed fixture as shown in Fig. 8b and 8c. This fixture eliminated the artifacts of the operator's hand during rotation and enabled smooth and controllable rotation of the glass capillary. Several design aspects were considered to achieve the 30 μm displacement resolution in the axial, lateral and vertical directions. A commercially-available luer-lock connector and a custom-designed holder on the fixture were used to minimize the axial movement of the flexible tubing, hence the glass capillary, during the manual rotation. This connector also facilitated easy connection of the glass capillary to the external suction source that was used for manipulating the worms. The glass capillary was also passed through a v-groove plate in between the luer-lock holder and the microfluidic device, that allowed minimizing its lateral displacement during the operation. The glass capillary was held inside the v-groove with the application of a vertical force via a top plate that was pushed against the capillary glass with a set of two compressed back-springs. The force exerted by the springs and the top plate was optimized to hold the glass capillary in the v-groove (eliminating vertical motions) while allowing its easy rotation for worm manipulation. To account for height mismatch between the fixed glass capillary and the microfluidic channel in various devices, we precisely controlled the thickness of the bottom PDMS layer in the device (at ~3.7 mm) and incorporated a levelling screw in the fixture that allowed us to adjust the height of the v-groove plate at desired

locations that corresponded precisely to each device. To demonstrate the necessity of the fixture, movement of the glass capillary tip inside the microfluidic device was measured in two different scenarios, i.e., with or without the 3D-printed fixture (Fig. 9a and 9b, respectively). Three different devices were tested for each scenario and the axial (ΔX) and lateral (ΔY) movements of the glass capillary tip were measured during 10 continuous rotations.

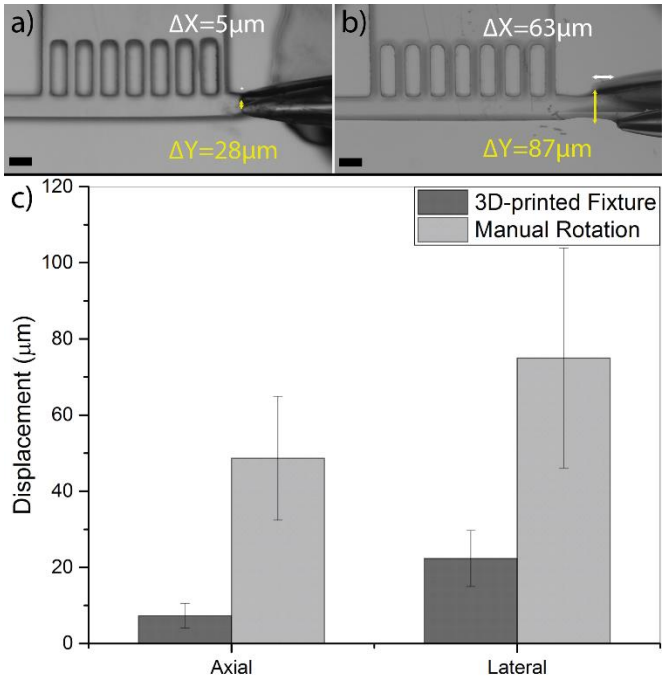

Figure 9: Axial (ΔX shown by white bars) and lateral (ΔY shown by yellow bars) displacements of the glass capillary tip inside the microfluidic device, shown by overlapping the capillary position on one image, when operated with (a) the 3D-printed fixture and (b) manually with no fixture. (c) Average and standard deviation of glass capillary tip displacement in lateral and axial directions when operated with 3D-printed fixture or manually inside N=3 different devices. Scale bar is 65µm.

Results in Fig. 9-c show a significant improvement in the lateral and axial displacement of the glass capillary tip inside the device when using the 3D-printed fixture to perform rotations. The average lateral and axial displacements reduced from 75±28 µm to 22±7 µm and from 48±16 µm to 7±3 µm, respectively, demonstrating that the use of fixture was necessary for continuation of our experiments. The small movements at the tip can be attributed to the 3D-printer resolution to produce smooth and flat surfaces as well as possible excess forces that may have been applied during the operation.

3.4.2 Single Worm Selection with Longitudinal Orientation

The single worm selection module had two major roles to play in our device, i.e., i) to orient worms longitudinally with heads towards the orientation and imaging channel, and ii) to select and load one worm at a time from the synchronized worm population into the imaging channel. For longitudinal orientation of worms, we utilized the natural preference of *C. elegans* to move towards the negative pole when exposed to electric field (electrotaxis) [49,73]. For this experiment, a population of young adult worms was loaded into the inlet channel of our device. To determine the efficiency of electrotactic longitudinal orientation approach, loaded animals were exposed to 2.6 V/cm electric field (optimum for young adult animals [49]) for 30 seconds after loading, then transferred with a 3 µl/sec flow rate towards the tapered microchannel at the entrance of the orientation and imaging channel. The longitudinal orientation of the worm that got trapped at the entrance of the tapered channel was then determined. A worm loaded with head was deemed as a successful longitudinal orientation. The results are shown in Fig. 10 in comparison with a

control group of animals that were not exposed to any electric field before loading into the tapered channel.

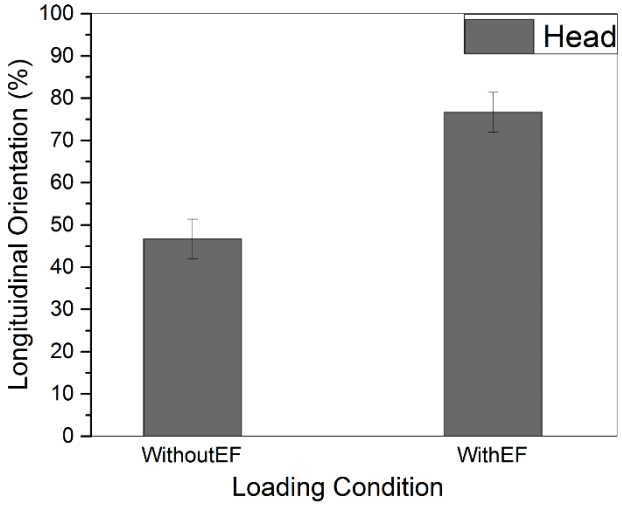

Figure 10: Longitudinal orientation of worms loaded into the tapered channel in the absence of electric field (WithoutEF, N=30 in 3 trials of 10 worms) or when the worms were exposed to electric field (WithEF, N=30 in 3 trials of 10 worms). Electrically-exposed worms showed an average of 76% head orientation after loading in comparison to 46% for the control group. Data shows average ± S.E.M

In the absence of electric field (WithoutEF group in Fig. 10), the longitudinal orientation of worms loaded into the tapered channel was random and resulted in an average success rate of 46±4.7% head orientation. Nevertheless, in the presence of electric field (WithEF group in Fig. 10), the average success rate in head orientation was increased to 76±4.7% of the worms. This shows the effectiveness of electrotactic method in proper longitudinal orientation of worms and their anterior loading into the orientation and imaging channel. Bordertaxis (attraction to surfaces) and positive rheotaxis (alignment

against fluid flow) [74] can be the causes of tail loading that dominated orientation of worms not exposed to electric field, but was overpowered by electrotaxis when an appropriate electric field was applied in the channel.

After obtaining the desirable longitudinal orientation of a worm and loading it into the tip of the tapered channel (Fig. 11a), other remaining worms that had been loaded into the inlet channel were washed out of the device so that only the captured worm would be retained for lateral orientation and imaging. For this purpose, worms were washed out to the recirculation channel with a 1 µl/sec flow of M9 buffer (Fig. 11b). The worm that was pre-loaded into the tapered channel remained in the device; this was because a hydrodynamic force was maintained at the back of the worm throughout the washing process. The recirculation channel was then closed (Fig. 11c) and the selected worm was loaded into the multidirectional orientation and imaging channel with a 3 µl/sec flow of M9 buffer (Fig. 11d). The process of selecting a worm, washing the device, and transferring the selected worm to the orientation and imaging channel took an average of 75 seconds and yielded a success rate of 76% for 30 animals tested.

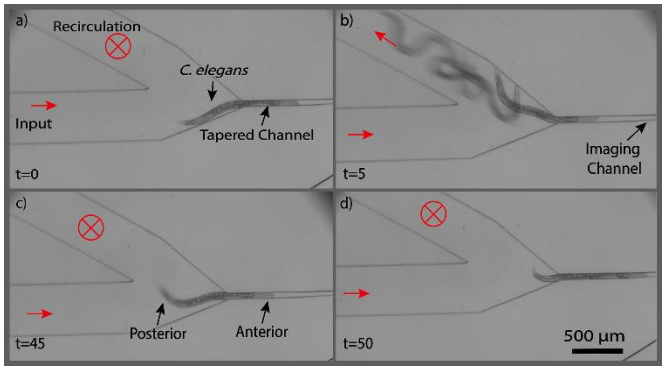

Figure 11: Time-lapse images of single worm selection after electrotactic longitudinal orientation in the device. (a) Single worm loaded into the trap after longitudinal orientation, (b) recirculation channel was opened and rest of the worms were washed out, (c) recirculation channel was closed, and (d) selected worm was inserted into the imaging module. Times are in seconds and red arrows indicate the flow direction in the channel.

3.4.3 Optimized Setting for Pneumatic Capturing of C. elegans

The single worm selection module allowed the user to longitudinally orient a population of worms in the device and load only one of them into the orientation and imaging channel. We desired to pneumatically manipulate (i.e., capture the head and rotate) the selected worm in this channel for multidirectional imaging of organs and neurons. The rotatable glass capillary, positioned at the end of the orientation and imaging channel (Fig. 7b) and connected to the regulated and pulsed suction source, was used to capture onto the worm's head and orient it laterally in the device. The duration and magnitude of the applied pneumatic force played an important role in manipulation of worms and had to be assessed and optimized first. In order to determine the optimum operation condition, that allowed for capturing the head of the worm without pulling too much of its body into the capillary, the effect of vacuum pressure (5, 10, and 15 psi) and pulsation frequency (continuous, 5

Hz, and 15 Hz) applied to the capillary was investigated for a time duration of 1 minute. The quality of manipulation was assessed by measuring the percentage of the worm's body remaining outside the glass capillary after 1 minute of pneumatic actuation as shown in Fig. 12a. Experiments were performed on N=10 animals at each actuation setting and the results are shown in Fig. 12b.

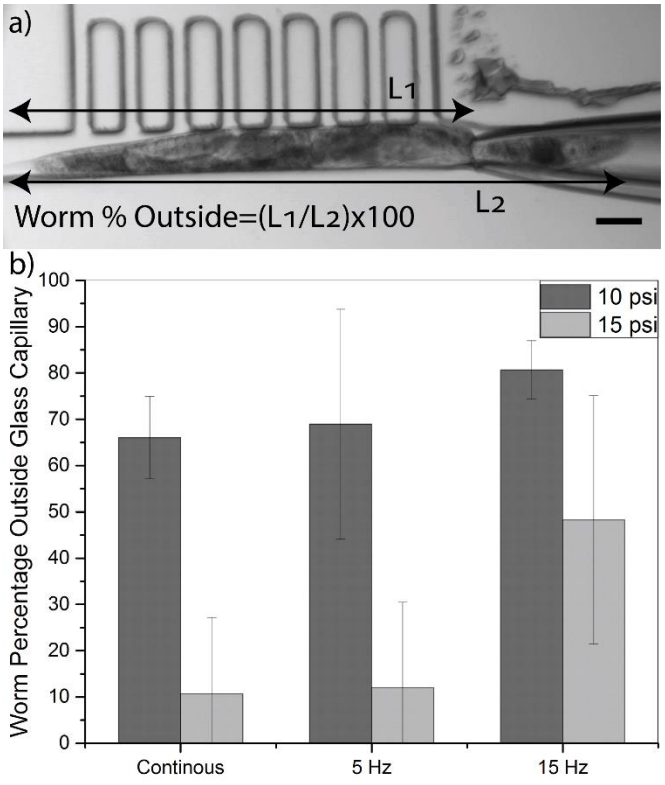

Figure 12: (a) Image (10x) taken after one-minute pneumatic manipulation of a young adult worm at 10 psi pressure pulsated at 5 Hz frequency. Worm percentage outside of the glass capillary was calculated as (L1/L2)×100. (b) Worm percentages (average ± S.E.M) outside the glass capillary manipulated with 10 and 15 psi vacuum pressures at different pulsation frequencies (continuous, 5 Hz, and 15 Hz) for 10 worms at each condition. Scale bar is 65µm.

A successful head capturing was defined as more than 70% of the worm's body being left outside the glass capillary after the one-minute pneumatic manipulation. When a 5 psi vacuum pressure was applied to the capillary, no matter what the pulsation frequency was, the captured worms were able to release their head from the glass capillary. Hence, manipulation was deemed unsuccessful at this pressure and not reported in Fig. 12b. At 15 psi vacuum pressure, more than half of the body was pulled into the glass capillary at continuous pressurization or under 5 Hz pulsation. Increasing the frequency to 15 Hz led to higher percentage (48%) of worms' body to be outside of the glass capillary. However, this setting was still not desirable for our purpose. At 10 psi vacuum pressure, less percentage of worms' body was pulled inside the glass capillary when compared to other pressure settings. On average, continuous mode and 5 Hz pulsation at 10 psi resulted in 66±8% and 68±24% of worms' body being left outside of the glass capillary, respectively. By increasing the frequency to 15 Hz, the average percentage of worms' body outside the glass capillary increased to 80±6%. This optimized setting (10 psi and 15 Hz) was used for pneumatic manipulation of worms for lateral orientation and multidirectional imaging in the rest of our experiments. Large error bars in some of the abovementioned experiments were resulted as worms were completely passing through the glass capillary during the manipulation. The variability in data is partially due to the worms' diameter differences in young adult stage as well as their subjective behaviour and body movement while being captured by the capillary.

3.4.4 Effect of Pneumatic Capturing on C. elegans Chemotaxis

In order to investigate the effect of glass capillary capturing on worms' post-orientation behavior, the chemotaxis assay was performed as described in the *Materials and Method* section. Approximately N=240 worms (in 4 triplicate trials) were captured for a minute with a glass capillary and then transferred to the food race plate. Fig. 13 shows the percentage of worms reaching the food colony at 10-minute intervals for the manipulated (with pneumatic capillary) and control worms. No significant difference was observed between the two groups of worms, indicating that pneumatic capturing had no effect on the worms' chemotaxis behavior when desirable pressure and pulsation conditions were applied.

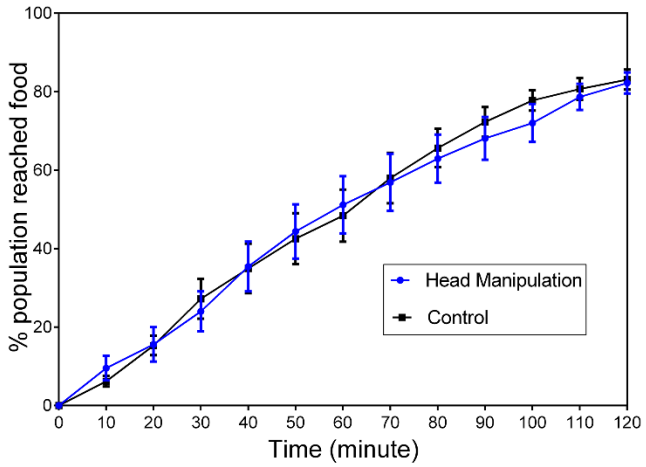

Figure 13: Chemotaxis assay (error bars showing S.E.M) for the worms that were captured pneumatically with a glass capillary for 1 min (blue)in comparison to the control worms that were not manipulated with the capillary glass (black). Experiment was performed in four trials, each in triplicate of approximately N=20 worms. No significant difference was observed between the head manipulation and control groups (two-way ANOVA test, P>0.5, effect size (r=η)=0.8)

3.4.5 Multi-Directional Orientation of C. elegans for Imaging of Organs and Neurons

We used our device to image neurons (ventral nerve cord or VNC) and vulva muscles (uv1& vulB1\2) of young adult *C. elegans* at different orientations as procedurally discussed in *Materials and Method* section. To be able to orient an unanesthetized and freely moving worm that had already been selected from a population (Fig. 11), the optimized setting for pneumatic head manipulation by the glass capillary (i.e., 10 psi pressure pulsed at 15 Hz) was employed. Manual rotation applied through the 3D-printed fixture (Fig. 8) provided controllable rotation of the capillary at only one degree of freedom. For demonstration purposes, images of a young adult worm were taken at three distinct orientations with 90 degree intervals as shown in Fig. 14. Both lateral (Fig. 14a-i and 14a-iii) and dorso-ventral (Fig. 14a-ii) orientations could be achieved conveniently. Typically, in a bright field image, the pharynx, gonads and vulva of the worm are distinguishable organs, which may be used as landmarks for determining different orientations. For example, as in Fig. 14a-i and Fig. 14a-iii, the lateral orientations of the worm were determined in reference to the side of the vulva (area directed by the red arrow). The vulva appears as an opening in the dorso-ventral orientation as shown in Fig. 14a-ii. To further validate the dorso-ventral orientation, the pharynx terminal bulb can also be utilized.

Upon successful demonstration of wild type strain orientation in the bright field mode, two other strains were used for fluorescent imaging of ventral and dorsal cord neurons, as well as vulval muscle cells. A strain expressing RFP in all neurons (pan-

neuronal RFP) was imaged as described above and various orientations are shown in Fig. 14-b. The VNC contains a larger bundle of neurites than the dorsal nerve cord (DNC); therefore, the VNC can be distinguished from the DNC based on the relative intensity of fluorescence. In addition to pan-neuronal imaging, we could also use our device to acquire GFP images of specific vulva muscle cells (uv1& vulB1\2) as shown in Fig. 14-c. The uv1 muscle cells were clearly visible at dorso-ventral orientation in comparison to two other lateral orientations. The VulB1\2 cells were distinguishable in all orientations with better spatial resolution in dorso-ventral orientation.

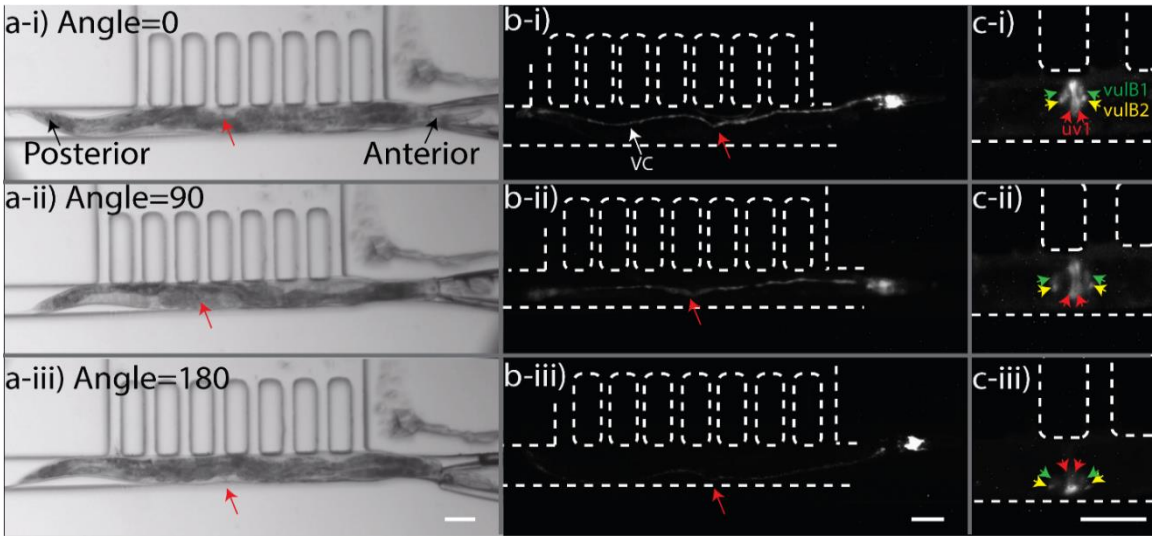

Figure 14: (a) Young adult worm bright field images at 90 degree intervals: i) lateral orientation (ventral side facing the suction channels), ii) dorso-ventral orientation (ventral side facing the imaging system) and iii) lateral orientation (ventral side facing the channel wall). Red arrows indicate the vulva. (b) RFP images of SGP14(sgpIs7) strain at 90° rotation intervals. Red arrows indicate the vulva. Ventral cord (VC) is shown with the white arrow in b-i. (c) GFP images of DY576 (lin-11::gfp) strain at 90° rotation intervals. Red arrows indicate uv1 cells. Green and yellow arrows indicate vulB1 and vulB2 respectively. All scale bars are 65µm (10x magnification).

With the optimized setting in our device, we were able to orient 30 freely moving animals with a 100% success rate while being able to pause orientation at any desired time and direction for imaging of organs and neurons as demonstrated in Fig. 14. Previously developed orientation techniques [62,65] can also manipulate worms in desired orientations; however, they require the worms to be chemically anesthetized. Chemical immobilization should preferably be avoided because anesthetics may have negative or inhibitory effects on worms' neuronal or behavioral processes that are sought in many applications. Our device could achieve orientation without the need for anesthetization but this was at the expense of reducing the throughput of experiments to account for voluntary movement and escape of worms. Another U-channel microfluidic passive orientation technique [60] could orient unanesthetized worms; however, orientation was only reported in the lateral direction. Our technique can orient unanesthetized worms at any desired orientation for further processing such as time-lapse chemical screening (not investigated). The angular resolution of orientation in our device can be significantly improved upon motorization of the glass capillary rotation in our device. Moreover, the overall throughput of the device can be significantly increased by computerization of processes such as selecting, capturing, orienting and releasing of the worm. This was not the focus of our work as we wanted to provide a semi-manual tool for easy adoption by the end users, but will be pursued in the next phase of research to develop a fully automated version of the microfluidic orientation device.

3.5 Conclusions

We have developed a hybrid microfluidic device to orient *C. elegans* at any desired longitudinal and lateral angle for imaging of organs, neurons, and cells. Worms could be laterally oriented with 76% success rate using their inherent electrotaxis response, then pneumatically captured with a glass capillary integrated inside the microfluidic device and orientated with 100% success in a narrow microchannel. A 3D-printed fixture was custom-designed to hold the microfluidic device and the glass capillary relatively fixed to each other, resulting in a smooth rotation of the capillary with lateral and axial displacement resolutions of 22 µm and 7 µm. The pneumatic capturing process was optimized in the device at 10 psi pressure pulsated at 15 Hz to prevent applying excessive forces to the worms. A chemotaxis assay on the captured worms demonstrated that this process does not negatively affect the behavior of worms in comparison to the ones that were not mechanically manipulated. Using the optimized manipulation settings, optical and fluorescent images of vulva and ventral cord as well as uv1, vulB1, and vulB2 cells could be successfully obtained with our device, which demonstrates its versatile application in *C. elegans* based studies. Our hybrid microfluidic device will facilitate investigating the muscle cells and neurons of unanesthetized worms at any desired orientation, in comparison to previously-reported orientation techniques which required anesthetized worms and were complex to provide post-orientation access to animals. In its current configuration, our device is ideal for chemical screening and monitoring of various biological processes in naturally inaccessible cells, neurons, and organs of unanesthetized

C. elegans. With design modifications, it can also be used in microinjection, electrophysiology, and laser ablation applications.

Chapter 4
Cardiac Screening of Intact *Drosophila melanogaster* Larvae under Exposure to Aqueous and Gaseous Toxins in a Microfluidic Device

4.1 Design and Fabrication of the Hybrid Microfluidic Screening Device

The hybrid microfluidic device (Fig. 15) was fabricated using the 3D printing method (Chapter 2) and consisted of two modules, i.e., animal handling module and chemical delivery module. The animal handling module consisted of loading and orientation glass capillaries (Fig. 15a) positioned at the front and end of an animal trap channel (Fig. 15b) which was equipped with four side suction channels (240 μm × 250 μm cross-section) for pneumatic immobilization of loaded larvae.

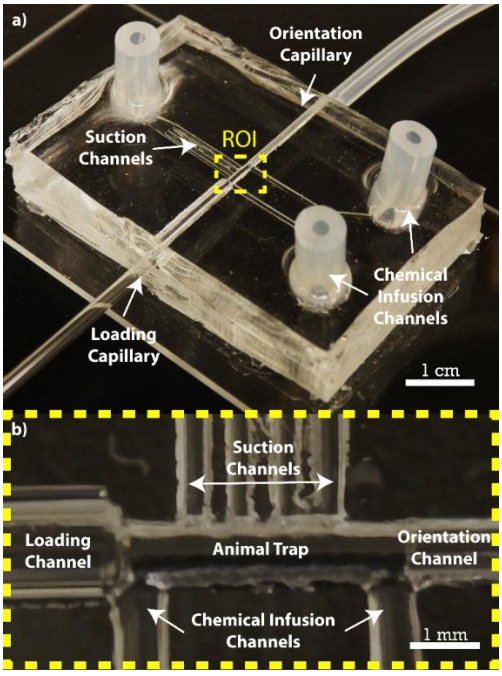

Figure 15: (a) Hybrid microfluidic chip used for 3rd instar Drosophila larva orientation, immobilization, chemical exposure, and monitoring of cardiac activities. Region of Interest (ROI) in (a) is magnified in (b). Loading and orientation glass capillaries were installed in the corresponding guide channels shown in (b) and rotated manually for larva orientation.

The loading glass capillary (1.1 mm inner diameter, Fisher Scientific, P# 22-260-943) was used to introduce 3rd instar *Drosophila* larvae individually from the PBS solution into the animal trap channel. This channel was 4 mm-long, 0.8 mm-wide, and 0.8 mm-thick and was intentionally designed to loosely conform to the early-stage 3rd instar *Drosophila* larva's body (0.6 mm diameter). The oversized trap design was implemented so that the loaded larva could be pneumatically captured from the head region using a negative pressure applied to the orientation glass capillary (0.4 mm inner diameter, Fisher Scientific, P# 1-000-0040) and rotated in the trap channel to achieve any favourable

orientation. The side suction channels were then used to achieve rapid immobilization of the oriented larva upon applying a negative pressure.

The chemical delivery module consisted mostly of external pneumatic tools (discussed in the next section) but also two chemical infusion channels (240 μm × 250 μm cross-section) placed at the side of the animal trap and opposite to the side suction channels (Fig. 15b). These channels were used to inject liquids and gases in Table 1 into desired spatial locations in the chip and towards the head or tail of the larva.

4.2 Experimental Setup and Procedure for *Drosophila* Orientation and Cardiac Screening

The designed hybrid microfluidic device (Fig. 15) was capable of loading, orienting, immobilizing, and monitoring the cardiac activities of 3rd instar *Drosophila melanogaster* larvae in a semi-automated manner. The experimental set-up (Fig. 16) that was used to operate the device and record the cardiac activities of the tested larvae consisted of three main components, i.e. the animal handling unit, the chemical delivery unit, and the monitoring and imaging unit. The animal handling unit consisted of two syringes connected to loading and orientation glass capillaries on the chip and a bench-top negative pressure source (regulated by a 0-15 psi vacuum gauge, Cole-Palmer, USA) connected to the side suction channels of the device. The chemical delivery unit consisted of a syringe pump (Legato 110, KD Scientific Inc., USA) for infusion of sodium azide or gas cylinders for introducing oxygen, carbon dioxide, air, or nitrogen into the device via the chemical infusion channels. Pressure regulators (0-145 psi, McMaster-Carr, USA) and

flow gauges (0.04-0.42 scfh, McMaster-Carr, USA) attached to the gas cylinders were used to adjust the volumetric flow rates of gases to desired levels (Table 1) before they were mixed in a T-junction and introduced into the device. The monitoring and imaging unit contained an inverted microscope (BIM-500FLD, Bioimager Inc., Canada), a camera (GS3-U3-23S6M-C, Point Grey Research Inc., Canada) and a computer for recording, storing and analysing the cardiac activities of tested larvae.

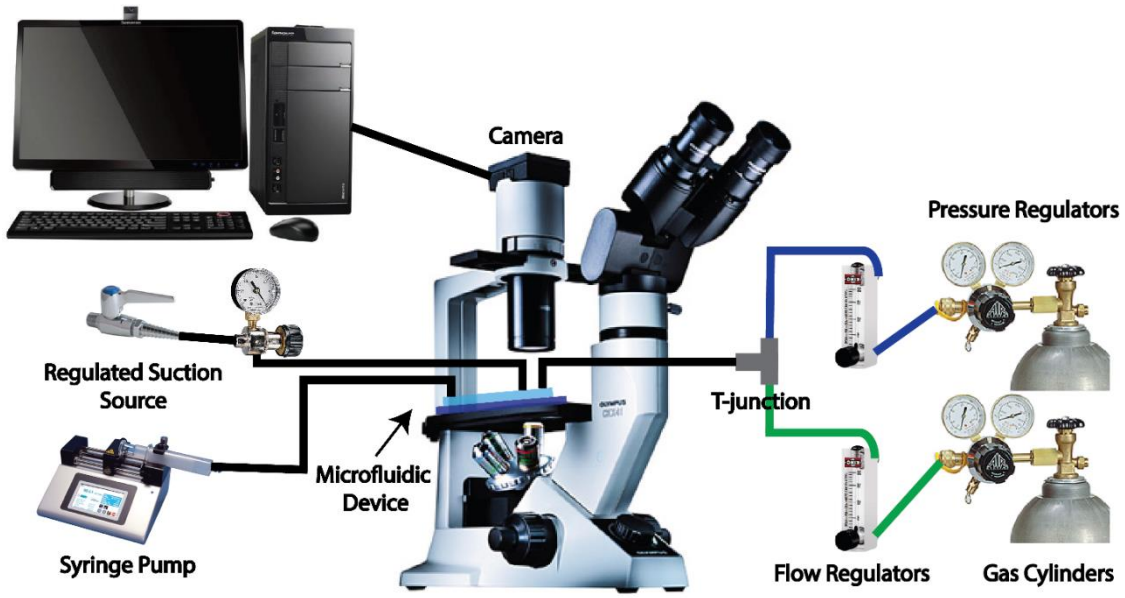

Figure 16: Experimental setup consisting of three main units, i.e., animal handling, chemical delivery, and monitoring and imaging units. Animal handling unit included two syringes connected to loading and orientation glass capillaries on the microfluidic device and a regulated suction source. Chemical delivery unit consisted of a syringe pump, gas cylinders, flow and pressure regulators, and a T-junction. Monitoring and imaging unit consisted of a microscope, a camera and a computer.

After preparation of the experimental setup and the animals, a 3rd instar *Drosophila* larva was selected and loaded into the loading glass capillary by applying a manual negative pressure. Loading capillary was then placed inside the microfluidic device via the

corresponding guide channel. The larva was introduced into the animal trap channel, captured pneumatically by the orientation glass capillary, and rotated in desired directions under the microscope. After achieving the desired dorsal orientation, regulated negative pressure (5-10 psi) was applied to the side suction channels to fully immobilize the oriented larva. A time duration of 5 minutes was provided to each animal at this point before recording the heartbeats in order to prevent recording of any deceptive heartbeats caused by stress. The heartrate activities were then monitored for the duration of the desired experiment at 30 frame per second (fps) recording speed. During these experiments and after a resting period of up to 5 minutes, different chemical stimuli at desired rates (1 ml min^{-1} for sodium azide and 50 ml min^{-1} for gases in Table 1) were introduced into the device via the chemical infusion channels. After an exposure duration of up to 10 minutes, the chemical stimulus was removed and the heart recovery was monitored for up to 3 minutes. Heartrates in Beats Per Minute (BPM) were then measured from the recorded videos by directly counting the movements of the trachea or heart [75] in 10 s intervals. These heartrates were normalized for each animal by dividing the measured values by the average heartrate of the animal one minute prior to exposure to chemical stimulus (called baseline heartrate). Tested animals were then removed from the device easily by using the loading glass capillary before the next animal was introduced into the chip for a new set of chemical screening.

4.3 Results and Discussions

Drosophila melanogaster is a promising model organism for cardiac diseases [26–29]. Nevertheless, cardiac studies on intact (alive and awake) *Drosophila* larvae poses a significant technological challenge that requires favourable orientation and full immobilization of the animal under the microscope with capability to expose the specimen to target chemicals with spatiotemporal accuracy. Hence, the application of intact larvae in cardiac toxicity assays has not been exploited to its full capacity. In order to monitor larva's cardiac activities under controllable exposure to chemicals, a hybrid microfluidic device (Fig. 15) was designed to desirably orient the larva and immobilize it thoroughly under the microscope, expose its posterior or anterior sides to various new chemicals (Table 1) with control over concentration and time, and analyze its transient heart activities during exposure and after removal of the chemical stimulus.

4.3.1 Intact Drosophila Larva Manipulation in the Hybrid Microfluidic Device

The hybrid microfluidic device, shown in Fig. 15, was operated as discussed in the previous section, under the Experimental Setup shown in Fig. 16. It enabled a minimally-trained operator to easily manipulate intact 3rd instar *Drosophila* larvae on the chip. A successful sample manipulation (Fig. 17) was defined as loading, orientation, and immobilization of a single animal for subsequent chemical exposure and cardiac investigations. A single larva suspended in PBS solution was loaded into the microfluidic device via the loading glass capillary (Fig. 17a). Longitudinal orientation of the larva inside

the chip was not a point of concern as the chip was designed with chemical infusion channels at the two ends of the animal trap to enable exposure of the larva from the head or tail regions as desired by the operator. Dorsal orientation (i.e., dorsal side of larva facing the microscope lens) was found to be necessary for successful acquisition of unobstructed videos from larva's heart. As such, the negative pressure in the orientation glass capillary was used to capture to the larva's head for subsequent lateral orientation. The captured larva was then rotated manually (Fig. 17b) by external rotation of the glass capillary to reach the desired dorsal orientation and to obtain the best possible visualization of the heart under the microscope. The oriented animal was then immobilized (Fig. 17c) by application of a 5-10 psi negative pressure to the side suction channels of the microfluidic device. A higher magnification image (5x in Fig. 17d) was then acquired in order to visualize and record the heartbeats clearly, for future quantitative assessment of cardiac activities.

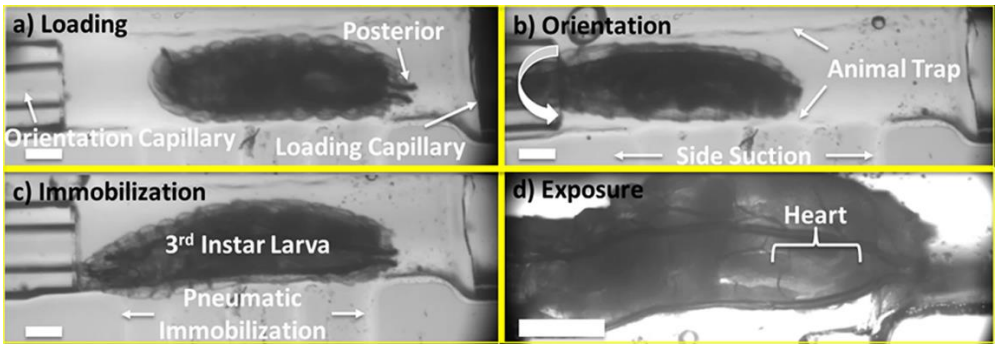

Figure 17: Intact 3rd instar Drosophila larva manipulation in the hybrid microfluidic device. The larva was (a) loaded from the loading glass capillary into the animal trap region of the chip, then (b) captured pneumatically by the orientation capillary and oriented dorsally under the microscope. It was then (c) immobilized via negative pressure in the side suction channels and (d) exposed to different chemicals while heartbeat activities were recorded at 5x magnification. Scale bars are all 250 µm.

A successful sample preparation took 3-4 minutes from animal selection in the stock bottle to immobilization in the chip. Animal unloading after immobilization was also achieved in less than a minute. The viability rate of N=10 larvae immobilized in the microfluidic device was found to be 90% (reaching adult stage) after ejection from the device as compared to 100% for control animals, which were not exposed to the device at all. Moreover, the chip could be used conveniently by minimally trained personnel to handle and manipulate *Drosophila* larvae. These provide significant advantages over the conventional larvae manipulation methods, in which tweezers are used to orient the larvae and anaesthetics, glue, or double-sided tape are used to immobilize them onto the substrate. Orientation with tweezers requires a high level of expertise and is highly prone to disruption of the cuticle while immobilization with glue or tape is irreversible and possibly toxic to the animals. Larvae manipulation in our device was easy, reversible, and did not require use of chemical reagents. In addition, this process may be accelerated by computer-based automation in the future.

4.3.2 Intact Drosophila Larvae Cardiac Activity Monitoring in the Hybrid Microfluidic Device

We aimed to use the microfluidic device for cardiac toxicity assays on intact *Drosophila* larvae under exposure to various new chemicals listed in Table 1. Hence, the effect of loading, orientation, and immobilization on animals' heart activity in the chip without any chemical exposure was investigated at this stage. Five 3rd instar *Drosophila* larvae were loaded individually into the microfluidic device, then oriented and

immobilized dorsally in the trap channel as shown in Fig. 17. Then, their heartrate was assessed at 5 minute intervals for a period of 20 minutes as discussed in the *Experimental Setup and Procedure* section. Another group of 3rd instar *Drosophila* larvae (N=5) were conventionally oriented with tweezers and immobilized with glue on a sylgard-coated substrate. Heartrate activities of the control group were also recorded and assessed in a similar manner. Fig. 18a demonstrates the heartrate of individual animals for both manipulation methods and the average heartrates are shown in Fig. 18b.

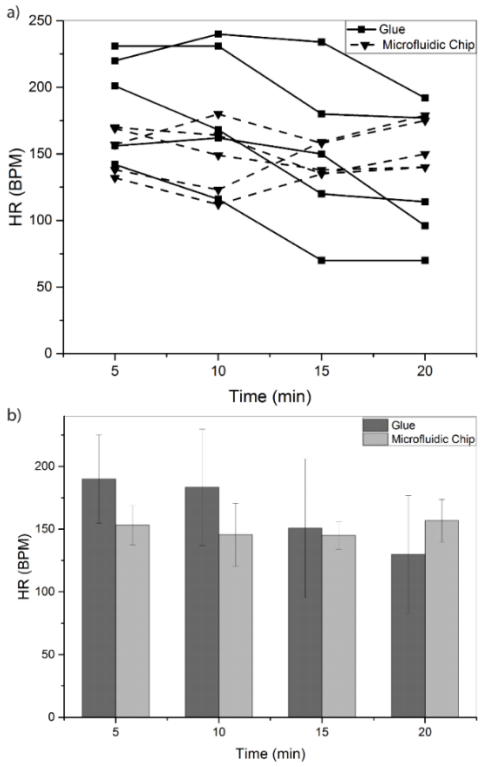

Figure 18: Heartrate (HR) activities of 3rd instar Drosophila larvae immobilized using the conventional glue-based (control group) method (N=5) and within the microfluidic device (N=5) for an immobilization period of 20 minutes. Heartrate of individual flies are shown in (a) while the average ± S.E.M. heartrates of all tested flies are shown in (b), demonstrating more stability over 20 min and less variability in heartrate for animals tested in the microfluidic device.

As shown in Fig. 18b, the initial heartrates in both methods (at t=5 min) were within the range of previously reported heartrates for intact larvae [76], which is known to be higher than the heartrate of dissected larvae [76]. Our statistical analysis of heartrate stability in the glue-based or microfluidic-based immobilization methods demonstrated no significant changes of heartrate with time (one-way ANOVA p-values of larger than 0.5). Further investigation of this phenomenon with a larger sample size is still required to draw a more confident conclusion. However, the conventional glue-based immobilization method resulted in an overall decline in the average heartrate values of the immobilized larvae while the microfluidic-based method resulted in a steadier cardiac activity over the immobilization period of 20 minutes. The variability of heartrate was also less significant between the animals immobilized in the microfluidic device. The decrease in the animals' heartrate immobilized by the glue can be attributed to the toxicity of the cyanoacrylate glue and its hyperthermia effect. Another disadvantage of the glue-based method in comparison to our technique is its irreversibility as per our discussions in previous section.

4.3.3 Cardiac Chemical Screening Assays using the Hybrid Microfluidic Device

Intact *Drosophila* larvae have not been adopted widely for cardiac toxicity assays mainly due to the complexities associated with precise exposure of animals to chemicals and visualizing their heart activities over extended periods of time (up to 20 minutes). As shown in previous section, the developed microfluidic device demonstrated no negative impact on the larvae heartbeat in this time period and provided a proper environment for

long-term assessment of individual larva's heart. This allowed us to use the chip for screening the effect of various aqueous and gaseous chemicals at different concentrations (Table 1) on the cardiac system of intact *Drosophila* larvae.

Concentration-Dependent Effect of Toxic Liquids on Cardiac Activities of Intact Drosophila Larvae.

Sodium azide (NaN_3) is one of the most widely used chemicals in various applications, such as pesticide production in agriculture industry [77], gas production in airbags in automotive industry [78], and mutagenesis or anesthesia in biological applications [79,80]. This chemical is believed to have severe toxicity effects on the brain and the heart; however, these effects are currently not well-understood [81–83]. *Drosophila melanogaster* larvae have been used as a model organism for toxicity and mutagenesis studies [80]. Here, we were interested to investigate whether intact 3rd instar *Drosophila* larva in our microfluidic chip can be used as a sensitive model to elucidate the immediate effect of sodium azide and its concentration on the cardiac system.

To investigate the effect of sodium azide on heart activities, 3rd instar *Drosophila* larvae were loaded into the microfluidic device and immobilized individually inside the trap as described in previous sections. Heart activities were recorded continuously in video formats for approximately 20 minutes. Animals were given 5 minutes to distress and then exposed to PBS for 10 minutes to stabilize in the device. The baseline heartrate used for data normalization was obtained at this time. The animals were then exposed to different concentrations of sodium azide solution (Table 1) at minute 10 with a flow rate of 1 ml

min^{-1} inside the two chemical infusion channels. As an example, one of the animals demonstrated a 188 BPM cardiac activity during the initial 10 min interval with no chemical, but after exposure to a 10% NaN_3 solution, a continuous reduction in the heartbeat was observed with values decreasing to 130, 24, and 0 BPM at 12, 15 and 18 minutes post exposure, respectively. The normalized heartrate activities for ten similarly-tested larvae at two different sodium azide concentrations (N=5 animals for each) are shown in Fig. 19.

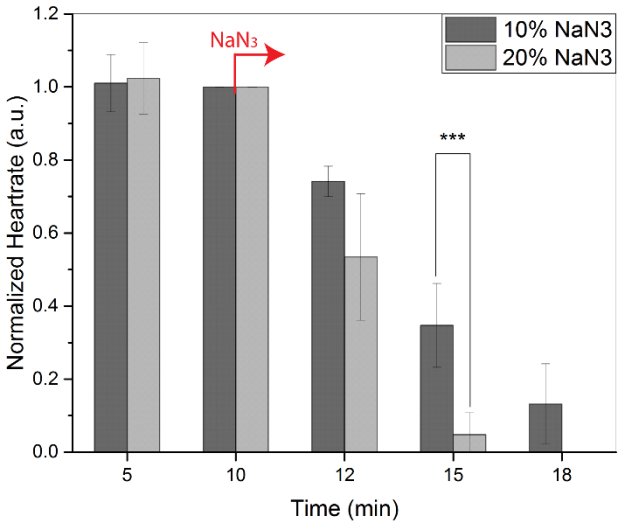

Figure 19: Normalized heartrate activities of 3rd instar intact Drosophila *larvae (N=5 for each exposure condition) under exposure to 10% and 20% sodium azide (NaN_3) solutions introduced at t=10 min past immobilization in the hybrid microfluidic device. t-Test statistical analysis at t=15 min resulted in a p-value of 3.5×10^{-3} ($p<0.01$) suggesting a significant difference in heartrate reduction rate between 10% and 20% NaN_3. a.u.: arbitrary unit*

As shown in Fig. 19, the immobilized larvae in the chip exposed to PBS for the beginning 10 minutes showed a stable heartrate activity (average 183±7 BPM). Upon introduction of 10% NaN_3 into the device at minute 10, heart activity reduced significantly

to 136±8 BPM at t=12 min and cardiac arrest was observed within 10 minutes of exposure. By increasing the concentration of NaN_3 to 20%, a faster rate of heartbeat reduction was observed (96±32 BPM at t=12 min) resulting in full stoppage of the heart within approximately 5 min after exposure to the chemical. The average heartrate values at t=15 min of exposure to 10% or 20% sodium azide were statistically different (p-value=3.5×10^{-3}, two-tailed t-test, d=2.92,1-β=0.47) proving that the concentration of chemical plays an important role in the rate of cardiac activity reduction. Spatial exposure of larvae's head or cuticle showed that sodium azide affected the heart activities very severely in both cases. No heartbeat recovery was observed for either concentrations after the removal of sodium azide and re-treatment of larvae with air. The results clearly demonstrated that sodium azide causes a severe cardiac arrest effect over a relatively short period of time on intact *Drosophila* larvae and further monitoring of the exposed larvae up to 24 hours post-exposure showed complete death of animals. The presented technology can, therefore, be conveniently used to investigate the biological pathways underlying the effect of sodium azide or other aqueous chemicals at any concentration on cardiac system of *Drosophila melanogaster* or other insects in their larval developmental stages.

Concentration-Dependent Effect of Toxic Gases on Cardiac Activities of Intact Drosophila Larvae.

Gaseous reagents, such as carbon dioxide and oxygen, are widely used in biological studies as anaesthetics or vital gases for living. The biological pathways involved in their sensing needs to be investigated systematically. For instance, it has been shown that carbon

dioxide can act as a chemo-attractant [84] or an anaesthetic chemical [37,40] in various insect species. Recent behavioural studies on *Drosophila* larvae [85,86] with different concentrations of oxygen proved that atypical soluble guanylyl cyclases (sGCs) act as oxygen sensors yet there are additional undefined proteins involved in this process that need to be investigated. The effects of hypoxia and re-oxygenation have also been recently studied on *Drosophila's* heart [87]. However, semi-intact (dissected) animals immersed in saline or artificial hemolymph solutions saturated with target gases have been mostly used in these studies and the immediate real-time heart responses under direct exposure to gases have not been investigated in intact animals. Our goal in this assay was to investigate the effect of concentration of oxygen (from anoxia to hyperoxia) or carbon dioxide (hypercapnia) on immediate and transient responses of intact *Drosophila* larva's heart, which was achievable with the hybrid microfluidic device introduced in this paper.

To achieve our goal, 3rd instar *Drosophila* larvae were oriented and immobilized individually inside the device and allowed to stabilize in heartrate while being exposed to environment air. Baseline heartrates were measured for a minute, then gases at desired concentrations (Table 1) were introduced at a flow rate of 50 ml min^{-1} towards the tail of the immobilized larva for 2 minutes. The gaseous stimulus was then removed and the heartrate recovery was investigated for another minute. For a single animal exposed to air (approximately 21% O_2 and 78% N_2) in Fig. 20a, no significant changes in heartrate activities were observed during the exposure as expected. Heartrate frequencies 30 seconds before exposure, during the 2-min exposure, and in the recovery period were all

approximately 180 BPM. For another larva exposed to 100% oxygen (hyperoxia) in Fig. 20b, slight increase in the heartrate activity during the exposure was observed. The heartrate increased from 180 BPM at 30 seconds before exposure to 198 BMP during exposure, which returned to 186 BPM at minute 4 upon the removal of oxygen from the device. In the anoxia experiment (0% oxygen) which is shown in Fig. 20c, the initial heartrate of the animal was 150 BPM at 30 seconds before exposure, which was rapidly reduced to 30 BMP during the 2-minutes exposure. Irregular periods of on and off beating was observed during the anoxia assay. However, rapid and full recovery of heart function (160 BMP heartrate at t=4 min) was observed upon introducing air back into the device. The overall normalized results (average ± S.E.M) for fifteen 3rd instar *Drosophila* larvae exposed to 0%, 21%, and 100% oxygen concentrations (N=5 animals for each concentration) are shown in Fig. 20.

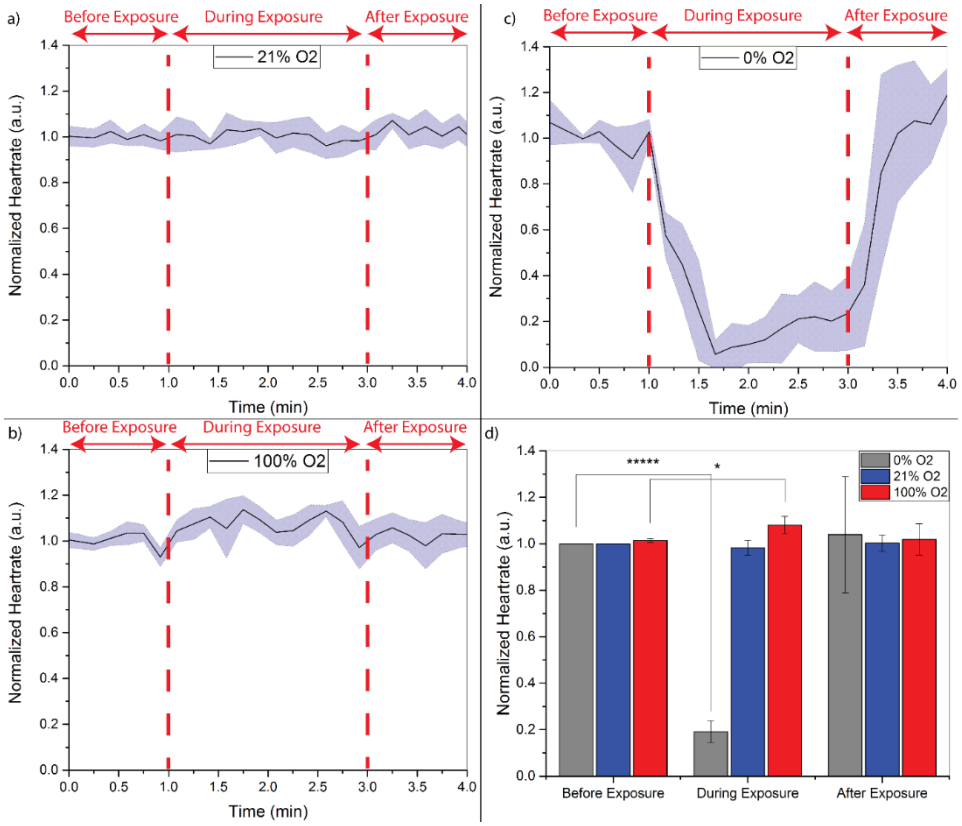

Figure 20: Normalized heartrate activities of 3rd instar intact Drosophila larvae (N=5 for each exposure condition) under exposure to oxygen (O_2) at (a) 21% (air), (b) 100% and (c) 0% (100% N_2) concentrations. Larvae's heartrates were monitored for a minute prior to exposure to obtain the baseline values for normalizing the data. The target gas was then introduced at t=1 min for two additional minutes. At t=3 min, the target gas was replaced by air and the heartrate recovery of larvae were quantitatively assayed. For this purpose, heartrates were counted in 10 s intervals and converted to heartrate frequency, then normalized by the baseline values. (d) Comparison of averaged normalized heartrate activities of assayed larvae at various time intervals (before, during, and after exposure) under exposure to 0%, 21% and 100% oxygen. For 100% O_2 exposure, a slight increase in heartrate activities was statistically identified with a p-value of 0.013 (using t-test) before and after exposure. T-test for 0% O_2 exposure resulted in a p-value of 2.7×10^{-6} suggesting a statistically significant decrease in heartrate. Data shows average ± S.E.M.

As shown in Fig. 20, heartrate activities remained relatively stable in the first minute of the assays and before any gases were introduced into the device (average of

180±8, 212±11, and 166±29 BPM for air, 100% O_2, and 0% O_2 concentrations, respectively). A steady heartrate activity was observed under exposure of larvae to 21% oxygen or pure air (Fig. 20a and 20d), showing that the flow of gas at 50 ml/min had no significant effect on the cardiac activities of larvae. This allowed us to study the effect of other concentrations of oxygen. During exposure of 100% oxygen (Fig. 20b), a 7% increase (227±7 BPM) in the averaged heartrate activities of larvae was observed (Fig. 20d). A two-tailed student's t-test on these results showed a p-value of 0.013 that indicated a small increase ($P<0.05$, $d=2.49$, $1-\beta=0.36$) in heartrate response of larvae to 100% oxygen. This is the first time that the cardiac response of intact *Drosophila* larvae to hyperoxia in a microdevice is reported, showing a similar slight increase in heartrate activities as observed in humans [88]. This increase in the heartrate can potentially be attributed to the toxic effect of free radicals of pure oxygen on the heart and tissues known as oxidative stress, which is common between vertebrates and invertebrates [89,90].

The effect of lack of oxygen or anoxia on cardiac activities of intact *Drosophila* larvae was more significant (Fig. 20c). The removal of oxygen from the device at t=1 min resulted in a rapid drop of heartrate (to 34 BPM) within the first 30 seconds and a short period of full heart stoppage in majority of the tested larvae. Interestingly, most animals gained a slow heartbeat after the sudden decline phase and continued to increase their heartrate with a very slow rate even during the anoxia phase. A t-test statistical analysis showed a significant effect ($p=2.7\times10^{-6}$, $d=24.24$ and $1-\beta=1$) of lack of oxygen on heartrate activities of intact *Drosophila* larvae. The increase in heartrate during anoxia was

continued with the slow rate until air was re-introduced into the device at minute 3. During this recovery phase, we observed that the rate of heartbeat increase in the animals improved significantly. All animals were able to fully recover to normal heartrate activity (199±19 BPM average heartrate) within 45 seconds of air exposure. To the best of our knowledge, this is the first time that the transient response of *Drosophila* larva under anoxia condition is investigated using a microfluidic device. The trends described above are similar to the ones observed in adult-stage flies under hypoxia conditions [91]. Hypoxia-inducible factor (HIF), the metabolic AMP-activated protein kinase, nitric oxide signalling pathways and trehalose [92] have all been shown to be involved in hypoxia and anoxia responses of mammalian heart cells, and are also present in *Drosophila* [93]. Our easy-to-use microfluidic device can facilitate anoxia, hypoxia, and hyperoxia studies in intact *Drosophila* larvae by reducing the time and expertise needed for cardiac studies, allowing for the quantification of cardiac activities in real-time, and enhancing the precision and sensitivity of the assays.

We also investigated the effect of carbon dioxide at two different concentrations (100% and 50%) on the heart activities of intact 3rd instar *Drosophila* larvae, following the same procedures discussed for oxygen experiments above. A longer recovery period of 2 minutes was provided to animals compared to the oxygen experiments due to the more severe effect of carbon dioxide on heart activities. For instance, for a larva immobilized in the device, the heartrate was 168 BPM right before exposure to carbon dioxide. However, upon exposing the larva to 100% carbon dioxide, the heartrate reduced to 48 BPM after 30

seconds and full stoppage was observed after 50 seconds. During the recovery phase, rapid heartrate increase to 156 BPM after a minute of re-exposure to air was observed. On the other hand, for a larva exposed to 50% carbon dioxide, heartrate reduced less rapidly from 156 BPM before exposure to 126 and 36 BPM within 30 s and 90 s of exposure, respectively. Full heartrate recovery to 168 BPM was observed within a minute after removing the 50% carbon dioxide stimulus. Overall normalized cardiac activity results for two groups of five larvae exposed to 50% and 100% carbon dioxide are shown and compared in Fig. 21.

The rate of heartrate decay in *Drosophila* larvae strongly depended on the concentration of carbon dioxide. Fig. 21a and 21c show a significant and rapid reduction in heartrate of animals after exposure to 100% carbon dioxide. The average heartrate for the five larvae right before exposure was 152±32 BPM, which was reduced to 10±18 BPM within 30 seconds after exposure. Full heart stoppage was variable across the tested larvae, ranging from 20 to 50 seconds. Compared to the anoxia assay (Fig. 20c) where animals gained a slight heartrate recovery during the lack of oxygen phase, no heartrate recovery was observed during exposure of animals to 100% carbon dioxide and after the full heart stoppage occurred. Interestingly, exposure to 50% carbon dioxide (Fig. 21b and 21c) resulted in a slower decay of heartrate and a full heart stoppage was only observed after 110 to 120 seconds post-exposure. The average heartrate for the five larvae before exposure to 50% CO_2 was 150±10 BPM, which was reduced to 114±13 and 66±15 BPM within 30 s and 90 s of exposure.

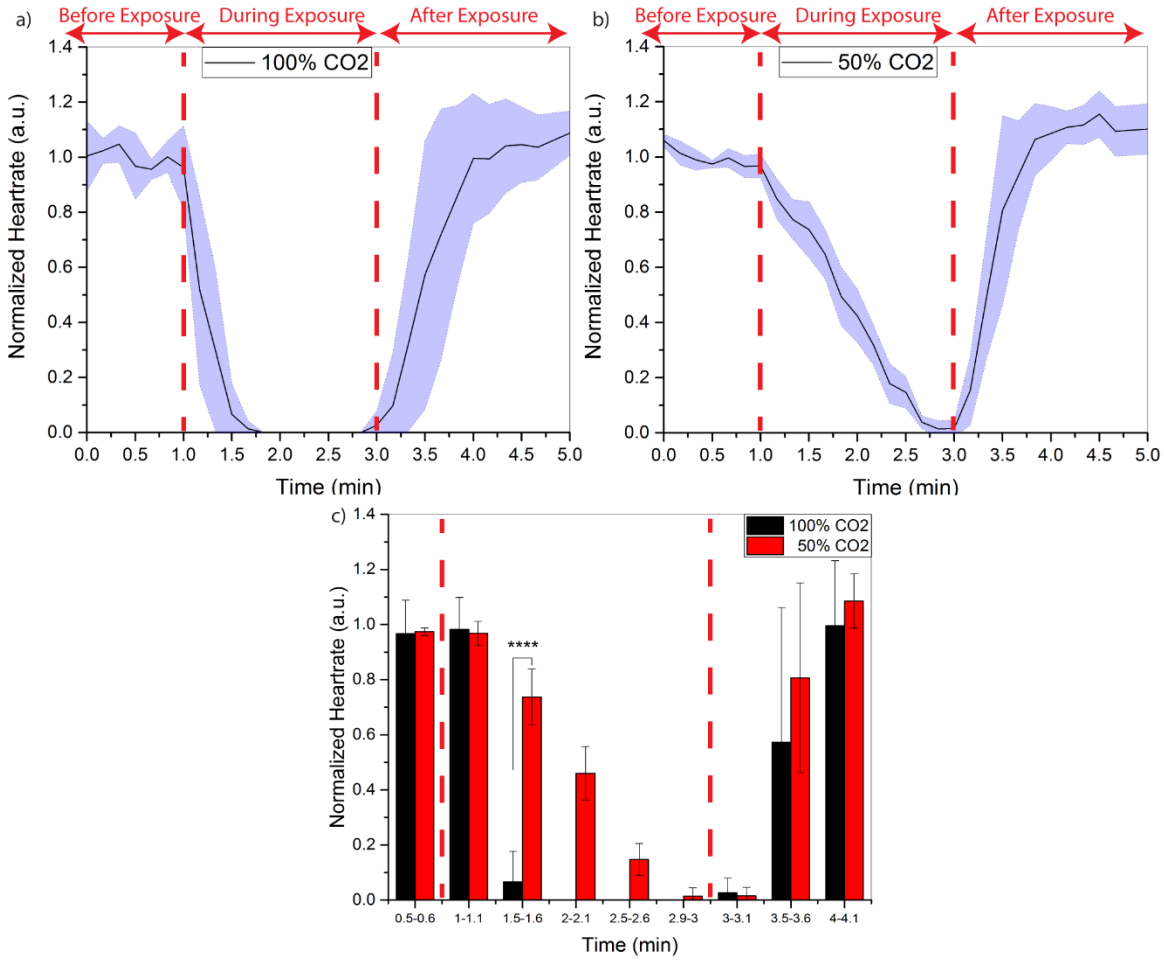

Figure 21: Normalized heartrate activities of 3rd instar intact Drosophila larvae (N=5 for each exposure condition) under exposure to carbon dioxide (CO_2) at (a) 100% and (b) 50% concentration levels. Larvae's heartbeats were monitored for a minute prior to exposure to obtain the baseline values for normalizing the data. The target gas was introduced at t=1 min for two additional minutes. At t=3 min, the target gas was replaced by air and the recovery of larvae were quantitatively assayed. For this purpose, heartrates were counted in 10 s intervals and converted to heartrate frequency, then normalized by the baseline values. (c) Comparison of averaged normalized heartrate activities of assayed larvae at various time intervals (before, during, and after exposure) under exposure to 100% and 50% carbon dioxide. t-Test statistical analysis at t=1.5-1.6 min resulted in a p-value of 3.8×10^{-5} ($p<0.0001$) suggesting a significant difference in heartrate reduction rate under exposure to various concentrations of CO_2. No significant difference during recovery phase ($p>0.05$) between difference concentrations was observed.

Statistical comparison between the two groups (Fig. 21c) after exposure to carbon dioxide showed a significant difference (t-test p-value of 3.8×10^{-5}, d=5.7 and 1-β=0.95) between the heartrate of animals within 30 seconds of exposure. After removal of the carbon dioxide stimulus, both group of animals recovered to a normal heartrate frequency with no significant difference in rate of recovery (Fig. 21c). The average heartrates after one minute of exposure to air were 146±26 and 163±12 BPM for 100% and 50% CO_2 conditions, respectively. However, a larger variability in heartrate was observed during the recovery phase of animals pre-exposed to 100% carbon dioxide as compared to 50%. This is potentially attributed to a more severe damage of carbon dioxide at higher concentrations on the heart that can be studied in the future. Our results in terms of the overall time of cardiac arrest under exposure to 100% carbon dioxide (Fig. 21a) and 100% nitrogen (Fig. 20c) are in agreement with Badre et al. [40]; however, our device enabled us to monitor real-time and transient cardiac activities of intact larvae under exposure to various concentrations of carbon dioxide and other gases for the first time.

4.4 Conclusions

Semi-intact or dissected *Drosophila melanogaster* larvae have been widely used for screening chemicals directly on the heart. A dissected larva maintained under synthetic hemolymph is physiologically unstable and not the ideal model for systemic chemical screening. Such investigations on intact animals are desirable but highly challenging due to the continuous locomotion of larva and the need for its immobilization as well as larva's semi-transparent cuticle and the need for orientation to obtain acceptable images of internal

organs such as heart. Conventional manipulation (e.g., tweezers) and immobilization (e.g., glue and tape) techniques are fatal to animals and irreversible. We have introduced a novel microfluidic device that can address all of the abovementioned challenges; hence, providing a platform technology for screening of chemicals in aqueous and gaseous phases directly on intact *Drosophila* larvae. The working principles can be applied identically with design modifications to develop microfluidic devices for screening other small-scale model organisms such as *C. elegans* and zebrafish.

Animals could be loaded and oriented easily inside our device by using integrated glass capillaries. Immobilization could also be achieved reversibly with no negative impact on the heart activities of *Drosophila* larvae. Elimination of image-obstructing glue allowed us to obtain clearer images of the heart in our device. Taking advantage of all these, we have investigated the cardiac response of intact *Drosophila* larvae to industrial chemicals such as sodium azide, carbon dioxide and oxygen. Concentration of these chemicals played a critical role in inducing hyper or hypo cardiac activities. Increased concentration of sodium azide and carbon dioxide led to a faster rate of decline in heartrate of animals until a full cardiac arrest was observed. Anoxia or lack of oxygen also led to a very rapid decline in cardiac activities but hyperoxia showed only a slight increase in the heartrate. Except for the exposure of sodium azide, animals were able to recover to a normal heartrate within a minute after removal of the stimuli with no significant effect from the pre-exposure condition.

Animal manipulation and screening can be done rapidly and reversibly with the presented device; however, in order to increase the throughput of this assay, some processes such as larva pneumatic capturing, glass capillary rotation, and video acquisition and analysis can be automated with pneumatic control setups, rotary motors, and video processing tools [94,95], respectively. The presented device can be used for investigation of biological pathways underlying cardiac responses and also for screening of various chemicals such as pharmaceutical, toxicological, and agricultural compounds on cardiac systems of intact *Drosophila melanogaster* or other compatible insect models. This will open new windows of opportunity in drug discovery and toxicology applications.

Chapter 5
Thesis Summary and Future Work

5.1 Thesis Summary

Model organisms, such as *C. elegans* and *D. melanogaster,* are used extensively in studying human diseases and screening chemicals for finding therapeutic drugs. Manipulation (i.e., orientation, immobilization, stimuli exposure, and neuronal or behavioral assessment) of these small-scale and actively-moving organisms is of great importance to biological assays. Conventional manipulation methods using hand-held tools require expertise and are time-consuming, thereby, they are not amenable to automation to achieve high throughput and accuracy in organism manipulation. Many microfluidic devices have been reported in the past decade for automated small-organism manipulation and assay. However, these microfluidic devices have not been capable of orienting unanesthetized organisms in all directions for biological assays. In other words, either the organisms had to be anesthetized to eliminate motion artifacts or their innate natural orientation (i.e., lateral) in the devices was studied. The technological gap in multi-directional manipulation of free-to-move *C. elegans* and *D. melanogaster* and post-manipulation screening needed to be addressed for further implementation of microfluidic devices in applications such as toxicology and drug discovery.

To address the need for manipulating unanesthetized small organisms, we used the concept of rotatable glass capillaries integrated inside polymeric microfluidic devices.

Glass capillaries with various inner diameters are widely available and can be accurately modified to match the size of the abovementioned model organisms. For instance, 30 μm and 400 μm ID glass capillaries were fabricated for *C. elegans* and *D. melanogaster* manipulation, respectively in our research. The general design of our device consisted of an inlet channel to load the organisms into an assay channel and an outlet channel to eject the animals after experiments. The rotatable glass capillary was integrated with the assay channel and used to pneumatically capture and orient the organisms prior to immobilization. Other components of a device were chemical exposure channels and imaging modules which were used to expose immobilized animals to different chemicals and image their responses at the neuron and/or organ levels.

Single organisms were selected from a synchronized population of randomly oriented animals, and loaded anteriorly into the assay trap of each device. The animal's head was first captured pneumatically via the glass capillary and, the pressure was subsequently altered to ensure that the body of the animal outside of the capillary is undamaged. A benefit to having most of the organism's body outside the glass capillary was the improvement of image quality since the glass capillary curvature distorts the images. *Drosophila* larva could be captured manually while a 10 psi pressure with 15 Hz pulsation was needed to capture adult *C. elegans.* 3D-printed fixtures were used to hold the glass capillary in place and provide controllable rotation to the captured animal. More precision was necessary for *C. elegans* orientation due to its small size (40-50 μm diameter) which

required much higher rotation resolution and accuracy in comparison to *Drosophila* larvae (0.6 mm diameter).

After achieving desirable orientation of small organisms in our devices, animals were further investigated to demonstrate the application of our sample preparation technique for post-orientation studies such as multi-directional imaging of *C. elegans* neurons or *Drosophila* heart under exposure to chemicals. Different strains of *C. elegans* were imaged inside the microfluidic device at 90 degrees intervals to visualize vulva and its associated muscles in brightfield and fluorescent modes, which are not clearly visible in the innate lateral orientation of the worm. After acquiring images, worms could be released and ejected through the output channel. For *Drosophila* screening, the larva was oriented dorsally, released, and then immobilized via the side suction channels while keeping the dorsal orientation. The larva's heart rate was monitored during exposure to various chemicals at different concentrations. Exposure to 10% and 20% sodium azide was found to caused unrecoverable stoppage of the heart at different cardiac arrest rates. Exposure to CO_2 gas also led to rapid and full arrest of the heart that was recovered after removal of the gas. With higher concentrations of toxic liquids or gases, our device was capable of detecting faster cardiac arrest rates in a sensitive manner. Different concentrations (0, 21 and 100%) of O_2 were also tested on *Drosophila*'s heart with our device. Lack of oxygen caused anoxia, which was observed as a rapid heart stoppage followed by slow heartrate recovery during the exposure. As expected, 21% O_2 (air) had no significant effect while

100% O_2 resulted in a 7% increase in the average heartrate of *Drosophila* larvae during exposure.

Our research successfully demonstrated the application of glass capillary-PDMS hybrid microfluidic devices for orienting and screening of unanesthetized *C. elegans* and *Drosophila* larvae. These devices can be used for chemical screening and monitoring of biological processes in *C. elegans* and *Drosophila* in unconventional orientations. For instance, biological pathways underlying cardiac responses of *Drosophila* to various chemicals can be investigated. Pertaining specifically to the agricultural industry, and developed pesticides can be screened to understand their effect on organs and cells of crop-invading insects. This screening devices can also facilitate drug discovery and toxicology studies by enabling end users to use model organisms of human diseases from different orientations to discover processes that are potentially not observable under organisms' natural orientation. The devices, with further iterations, can be implemented for applications in microinjection, electrophysiology, and laser ablation in both model organisms.

5.2 Future Work

In the *C. elegans* device presented the side suction channels for immobilizing worms after orientation was challenging to operate. Animals were pulled through the narrow channels by the side suction force during our experiments. To address this challenge, the height of side suction channels should be made smaller (i.e., 10-30 μm) than the diameter of young adult *C. elegans* (40-50 μm). The lower height of suction channels

would create a vacuum seal for *C. elegans* immobilization as previously reported [54] while same size or larger channels would result in excessive liquid withdrawal and animal being suctioned into the channel. To fabricate such a device, two-step photolithography is needed to provide two different heights for the side suction channels and the rest of the device.

Upon immobilizing the worms in the channel, a variety of chemicals can be tested similarly to the method shown for *Drosophila* model. This opens a new window for application of our device to conduct drug screening and toxicology studies using *C. elegans*. Moreover, previously developed microfluidic techniques for laser ablation and microsurgery [96] on worms lack the orientation capability, and hence unable to perform surgery at unconventional locations. With implementation of our device, laser ablation of specific neurons and microsurgery of specific cells can be performed with more precision.

The developed orientation technique can also be used in microinjection of *C. elegans* or *Drosophila* embryos to produce transgenic mutants. Proper orientation of unanesthetized *C. elegans* is crucial as the DNA should be injected into the worm's gonad. With the current manual microinjection method, a large number of attempts has to be made to achieve a successful injection for obtaining the transgenic strains. Few microfluidic devices have been developed to automate the microinjection process through automatic animal loading and motorized x-y axis needle locator to inject desired site of the worm [54,55]. However, their success rate in producing transgenic animals is either very low or not reported at all. As a microfluidic design restriction, the needle has to be located

permanently on one side of the channel. To achieve a successful microinjection, the worm's gonad can be rotated using our orientation module to face the microneedle. The microneedle can also be connected to a micromanipulator and an accurate pump to facilitate precise penetration of needle into the gonad and release of RNA for obtaining the desired transgenic strains with higher success rate and throughput.

Another avenue to explore with our orientation method is to obtain 3D images of neuronal morphology or body anatomy of different model organisms and their transgenic mutants. As explained in the introduction chapter, variety of mutants can be developed experimentally which requires performing multidirectional imaging to determine the success and accuracy of the developed mutant. Currently, expensive techniques such as confocal microscopy are used for 3D imaging of organisms. With our technique, images from various orientations can be obtained and assembled using a software to generate 3D images of desired body parts and potentially cells and neurons. Automation of organism rotation, image acquisition and image processing is of great importance to achieve this objective. Lower-cost 3D imaging modules can help end users in various biological studies such as discovery of new mutant lines of *C. elegans* and *D. melanogaster*.

In order to achieve ideal high throughput organism manipulation, the processes of loading, orientation, immobilization, and ejection of organisms must be automated. Loading and ejection can be automated by solenoid actuators and deformable membrane valves to automate the fluid flow in the microchannels as shown in various publications [45,55,60]. Orientation can be automated by using a stepper motor to rotate the glass

capillary and integrating a real-time image processing unit to determine the correct orientation of the organism. These implementations can lead to development of fully automated chemical screening microdevices, capable of performing assays and gathering results without the continuous involvement of an operator. The applications of such devices are extremely broad as discussed in this thesis.

References

[1] Guarente, L., and Kenyon, C., 2000, "Genetic pathways that regulate ageing in model organisms.," Nature, **408**(6809), pp. 255–262.

[2] Hartwell, L. H., Szankasi, P., Roberts, C. J., Murray, A. W., and Friend, S. H., 1997, "Integrating Genetic Approaches into the Discovery of Anticancer Drugs," Science, **278**(5340), pp. 1064–1068.

[3] Hendricks, J. C., Sehgal, A., and Pack, A. I., 2000, "The need for a simple animal model to understand sleep," Prog. Neurobiol., **61**(4), pp. 339–351.

[4] Manev, H., and Dimitrijevic, N., 2004, "Drosophila model for in vivo pharmacological analgesia research.," Eur. J. Pharmacol., **491**(2-3), pp. 207–8.

[5] Manev, H., and Dimitrijevic, N., 2005, "Fruit flies for anti-pain drug discovery.," Life Sci., **76**(21), pp. 2403–7.

[6] de Bono, M., and Maricq, A. V., 2005, "Neuronal substrates of complex behaviors in C. elegans.," Annu. Rev. Neurosci., **28**, pp. 451–501.

[7] Medioni, C., Sénatore, S., Salmand, P.-A., Lalevée, N., Perrin, L., and Sémériva, M., 2009, "The fabulous destiny of the Drosophila heart.," Curr. Opin. Genet. Dev., **19**(5), pp. 518–25.

[8] Jeibmann, A., and Paulus, W., 2009, "Drosophila melanogaster as a model organism of brain diseases," Int. J. Mol. Sci., **10**(2), pp. 407–440.

[9] C. elegans sequencing consortium, 1998, "Genome sequence of the nematode C. elegans: a platform for investigating biology.," Science, **282**(5396), pp. 2012–2018.

[10] Reiter, L. T., Potocki, L., Chien, S., Gribskov, M., and Bier, E., 2001, "A Systematic Analysis of Human Disease-Associated Gene Sequences In Drosophila melanogaster," Genome Res., **11**, pp. 1114–1125.

[11] Kaletta, T., and Hengartner, M. O., 2006, "Finding function in novel targets: C. elegans as a model organism.," Nat. Rev. Drug Discov., **5**(5), pp. 387–98.

[12] Pandey, U. B., and Nichols, C. D., 2011, "Human Disease Models in Drosophila melanogaster and the Role of the Fly in Therapeutic Drug Discovery," Drug

Deliv., **63**(2), pp. 411–436.

[13] Jiang, S. Y., and Ramachandran, S., 2010, "Natural and artificial mutants as valuable resources for functional genomics and molecular breeding," Int. J. Biol. Sci., **6**(3), pp. 228–251.

[14] Riddle, D. L., Blumenthal, T., Meyer, B. J., and Priess, J. R., 1997, "C. elegans II," Cold Spring Harbor (NY): Cold Spring Harbor Laboratory Press.

[15] Salam, S., Ansari, A., Amon, S., Rezai, P., Selvaganapathy, P. R., Mishra, R. K., and Gupta, B. P., 2013, "A microfluidic phenotype analysis system reveals function of sensory and dopaminergic neuron signaling in C. elegans electrotactic swimming behavior.," Worm, **2**(September), p. e24558.

[16] Nass, R., Hall, D. H., Miller, D. M., and Blakely, R. D., 2002, "Neurotoxin-induced degeneration of dopamine neurons in Caenorhabditis elegans.," Proc. Natl. Acad. Sci. U. S. A., **99**(5), pp. 3264–3269.

[17] Adams, M. D., Celniker, S. E., Holt, R. A., and Al., E., 2000, "The genome sequence of Drosophila melanogaster.," Science, **287**(5461), pp. 2185–2195.

[18] Boyle, J., and Cobb, M., 2005, "Olfactory coding in Drosophila larvae investigated by cross-adaptation.," J. Exp. Biol., **208**(Pt 18), pp. 3483–91.

[19] Carey, A. F., and Carlson, J. R., 2011, "Insect olfaction from model systems to disease control.," Proc. Natl. Acad. Sci. U. S. A., **108**(32), pp. 12987–12995.

[20] Keene, A. C., and Waddell, S., 2007, "Drosophila olfactory memory: single genes to complex neural circuits.," Nat. Rev. Neurosci., **8**, pp. 341–354.

[21] O'Kane, C. J., 2011, "Drosophila as a model organism for the study of neuropsychiatric disorders," Molecular and functional models in neuropsychiatry, Springer, pp. 37–60.

[22] Lenz, S., Karsten, P., Schulz, J. B., and Voigt, A., 2013, "*Drosophila* as a screening tool to study human neurodegenerative diseases," J. Neurochem., **127**(4), pp. 453–460.

[23] Leung, C., Wilson, Y., Khuong, T. M., and Neely, G. G., 2013, "Fruit flies as a powerful model to drive or validate pain genomics efforts.," Pharmacogenomics, **14**(15), pp. 1879–87.

[24] Donelson, N. C., and Sanyal, S., 2015, "Use of Drosophila in the investigation of

Sleep Disorders.," Exp. Neurol., **274**, pp. 72–79.

[25] Fujiwara, M., Hamatake, Y., Arimoto, S., Okamoto, K., Suzuki, T., and Negishi, T., 2011, "Exposure to Cigarette Smoke Increases Urate Level and Decreases Glutathione Level in Larval Drosophila melanogaster," Genes Environ., **33**(3), pp. 89–95.

[26] Gu, G. G., and Singh, S., 1995, "Pharmacological analysis of heartbeat in Drosophila.," J. Neurobiol., **28**(3), pp. 269–80.

[27] Ocorr, K., Perrin, L., Lim, H.-Y., Qian, L., Wu, X., and Bodmer, R., 2007, "Genetic control of heart function and aging in Drosophila.," Trends Cardiovasc. Med., **17**(5), pp. 177–182.

[28] Diop, S. B., and Bodmer, R., 2012, "Drosophila as a model to study the genetic mechanisms of obesity-associated heart dysfunction," J. Cell. Mol. Med., **16**(5), pp. 966–971.

[29] Qian, L., and Bodmer, R., 2012, "Probing the polygenic basis of cardiomyopathies in Drosophila," J. Cell. Mol. Med., **16**(5), pp. 972–977.

[30] Ocorr, K., Vogler, G., and Bodmer, R., 2014, "Methods to assess Drosophila heart development, function and aging.," Methods, **68**(1), pp. 265–72.

[31] Altun, Z. F., and Hall, D. H., 2016, "Introduction to c. elegans anatomy," Handb. C. elegans Anatomy. WormAtlas. [Online]. Available: http://www.wormatlas.org/hermaphrodite/hermaphroditehomepage.htm.

[32] Bob Argiropoulos, "Drosophila Development" [Online]. Available: http://www.zoology.ubc.ca/~bio463/lecture_13.htm.

[33] Chung, S. H., and Mazur, E., 2009, "Femtosecond laser ablation of neurons in C. elegans for behavioral studies," Appl. Phys. A, **96**(2), pp. 335–341.

[34] Cooper, A. S., Rymond, K. E., Ward, M. A., Bocook, E. L., and Cooper, R. L., 2009, "Monitoring heart function in larval Drosophila melanogaster for physiological studies.," J. Vis. Exp., (33), pp. 1–6.

[35] Zhang, M., Chung, S. H., Fang-Yen, C., Craig, C., Kerr, R. a., Suzuki, H., Samuel, A. D. T., Mazur, E., and Schafer, W. R., 2008, "A Self-Regulating Feed-Forward Circuit Controlling C. elegans Egg-Laying Behavior," Curr. Biol., **18**(19), pp. 1445–1455.

[36] Mondal, S., Ahlawat, S., Rau, K., Venkataraman, V., and Koushika, S. P., 2011, "Imaging in vivo neuronal transport in genetic model organisms using microfluidic devices.," Traffic, **12**(4), pp. 372–85.

[37] Ghannad-Rezaie, M., Wang, X., Mishra, B., Collins, C., and Chronis, N., 2012, "Microfluidic chips for in vivo imaging of cellular responses to neural injury in Drosophila larvae.," PLoS One, **7**(1), p. e29869.

[38] Mello, C. C., Kramer, J. M., Stinchcomb, D., and Ambros, V., 1991, "Efficient gene transfer in C.elegans: extrachromosomal maintenance and integration of transforming sequences.," EMBO J., **10**(12), pp. 3959–3970.

[39] Goodman, M. B., Lindsay, T. H., Lockery, S. R., and Richmond, J. E., 2012, "Electrophysiological Methods for C. elegans Neurobiology," Methods Cell Biol, **107**, pp. 409–436.

[40] Badre, N. H., Martin, M. E., and Cooper, R. L., 2005, "The physiological and behavioral effects of carbon dioxide on Drosophila melanogaster larvae.," Comp. Biochem. Physiol. A. Mol. Integr. Physiol., **140**(3), pp. 363–376.

[41] Wlodkowic, D., Khoshmanesh, K., Akagi, J., Williams, D. E., and Cooper, J. M., 2011, "Wormometry-on-a-chip: Innovative technologies for in situ analysis of small multicellular organisms," Cytom. Part A, **79A**(10), pp. 799–813.

[42] Yang, F., Gao, C., Wang, P., Zhang, G.-J., and Chen, Z., 2016, "Fish-on-a-chip: microfluidics for zebrafish research.," Lab Chip, **16**(7), pp. 1106–25.

[43] Gupta, B., and Rezai, P., 2016, "Microfluidic Approaches for Manipulating, Imaging, and Screening C. elegans," Micromachines, **7**(7), p. 123.

[44] Han, B., Kim, D., Ko, U. H., Shin, J. H., Hyun Ko, U., and Shin, J. H., 2012, "A sorting strategy for C. elegans based on size-dependent motility and electrotaxis in a micro-structured channel.," Lab Chip, **12**(20), pp. 4128–34.

[45] Rohde, C. B., Zeng, F., Gonzalez-Rubio, R., Angel, M., and Yanik, M. F., 2007, "Microfluidic system for on-chip high-throughput whole-animal sorting and screening at subcellular resolution.," Proc. Natl. Acad. Sci. U. S. A., **104**(35), pp. 13891–5.

[46] Ai, X., Zhuo, W., Liang, Q., McGrath, P. T., and Lu, H., 2014, "A high-throughput device for size based separation of C. elegans developmental stages.," Lab Chip, **14**(10), pp. 1746–52.

[47] Shi, W., Wen, H., Lin, B., and Qin, J., 2011, “Microfluidic platform for the study of caenorhabditis elegans,” Top. Curr. Chem., **304**, pp. 323–338.

[48] Hulme, S. E., Shevkoplyas, S. S., McGuigan, A. P., Apfeld, J., Fontana, W., and Whitesides, G. M., 2010, “Lifespan-on-a-chip: microfluidic chambers for performing lifelong observation of C. elegans.,” Lab Chip, **10**(5), pp. 589–97.

[49] Rezai, P., Siddiqui, A., Selvaganapathy, P. R., and Gupta, B. P., 2010, “Electrotaxis of Caenorhabditis elegans in a microfluidic environment.,” Lab Chip, **10**(2), pp. 220–226.

[50] Rezai, P., Siddiqui, A., Selvaganapathy, P. R., and Gupta, B. P., 2010, “Behavior of Caenorhabditis elegans in alternating electric field and its application to their localization and control,” Appl. Phys. Lett., **96**(15).

[51] Rezai, P., Salam, S., Selvaganapathy, P. R., and Gupta, B. P., 2011, “Effect of pulse direct current signals on electrotactic movement of nematodes Caenorhabditis elegans and Caenorhabditis briggsae,” Biomicrofluidics, **5**(4), pp. 44116–441169.

[52] Lockery, S. R., Hulme, S. E., Roberts, W. M., Robinson, K. J., Laromaine, A., Lindsay, T. H., Whitesides, G. M., and Weeks, J. C., 2012, “A microfluidic device for whole-animal drug screening using electrophysiological measures in the nematode C. elegans.,” Lab Chip, **12**(12), pp. 2211–20.

[53] Hu, C., Dillon, J., Kearn, J., Murray, C., O’Connor, V., Holden-Dye, L., and Morgan, H., 2013, “NeuroChip: a microfluidic electrophysiological device for genetic and chemical biology screening of Caenorhabditis elegans adult and larvae.,” PLoS One, **8**(5), p. e64297.

[54] Zhao, X., Xu, F., Tang, L., Du, W., Feng, X., and Liu, B., 2013, “Microfluidic chip-based C. elegans a system for investigating cell–cell communication in vivo,” Biosens. Bioelectron., **50**, pp. 28–34.

[55] Song, P., Dong, X., and Liu, X., 2016, “A microfluidic device for automated, high-speed microinjection of Caenorhabditis elegans,” Biomicrofluidics, **10**, p. 011912.

[56] Ghannad-Rezaie, M., Wang, X., Mishra, B., Collins, C., and Chronis, N., 2011, “Microfluidic Chip for Immobilizing and in Vivo Imaging of Drosophila Larvae,” PLoS One, **7**(1), p. e29869.

[57] Ghaemi, R., Rezai, P., Iyengar, B. G., and Selvaganapathy, P. R., 2015, “Microfluidic devices for imaging neurological response of Drosophila

melanogaster larva to auditory stimulus," Lab Chip, **15**(4), pp. 1116–1122.

[58] Yanik, M. F., Rohde, C. B., and Pardo-Martin, C., 2011, "Technologies for micromanipulating, imaging, and phenotyping small invertebrates and vertebrates.," Annu. Rev. Biomed. Eng., **13**, pp. 185–217.

[59] Crane, M. M., Chung, K., Lu, H., Stirman, J., and Lu, H., 2010, "Microfluidics-enabled phenotyping, imaging, and screening of multicellular organisms.," Lab Chip, **10**(12), pp. 1509–1517.

[60] Cáceres, I. D. C., Valmas, N., Hilliard, M. a, and Lu, H., 2012, "Laterally orienting C. elegans using geometry at microscale for high-throughput visual screens in neurodegeneration and neuronal development studies.," PLoS One, **7**(4), p. e35037.

[61] Fauver, M., Seibel, E., Rahn, J. R., Meyer, M., Patten, F., Neumann, T., and Nelson, A., 2005, "Three-dimensional imaging of single isolated cell nuclei using optical projection tomography.," Opt. Express, **13**(11), pp. 4210–23.

[62] Rieckher, M., Birk, U. J., Meyer, H., Ripoll, J., and Tavernarakis, N., 2011, "Microscopic optical projection tomography in vivo.," PLoS One, **6**(4), p. e18963.

[63] Pardo-Martin, C., Allalou, A., Medina, J., Elimon, J., Wählby, C., and Yanik, M. F., 2013, "High-throughput hyperdimensional vertebrate phenotyping," Nat. Commun., (4), p. 1467.

[64] Petzold, A., Bedell, V., Boczek, N., Essner, J., Balciunas, D., Clark, K., and Ekker, S., 2010, "SCORE imaging: specimen in a corrected optical rotational enclosure," Zebrafish, **7**(2), pp. 149–154.

[65] Ahmed, D., Ozcelik, A., Bojanala, N., Nama, N., Upadhyay, A., Chen, Y., Hanna-Rose, W., and Huang, T. J., 2016, "Rotational manipulation of single cells and organisms using acoustic waves," Nat Commun, **7**, pp. 1–11.

[66] Hulme, S. E., Shevkoplyas, S. S., Apfeld, J., Fontana, W., and Whitesides, G. M., 2007, "A microfabricated array of clamps for immobilizing and imaging C. elegans.," Lab Chip, **7**(11), pp. 1515–23.

[67] Chokshi, T. V., Ben-Yakar, A., and Chronis, N., 2009, "CO2 and compressive immobilization of C. elegans on-chip.," Lab Chip, **9**(1), pp. 151–7.

[68] Chung, K., and Lu, H., 2009, "Automated high-throughput cell microsurgery on-chip.," Lab Chip, **9**(19), pp. 2764–6.

[69] Mondal, S., Ahlawat, S., and Koushika, S. P., 2012, “Simple microfluidic devices for in vivo imaging of C. elegans, Drosophila and zebrafish.,” J. Vis. Exp., (67), pp. 1–9.

[70] Pullers, P.-M., 2015, Pipette Cookbook 2015 (P-97 & P-1000 Micropipette Pullers), Sutter Instrument Company.

[71] Soper, D., “Statistics Calculators [version 4.0]” [Online]. Available: http://www.danielsoper.com/statcalc/default.aspx. [Accessed: 19-Aug-2016].

[72] Sullivan, G. M., and Feinn, R., 2012, “Using Effect Size - or Why the P Value Is Not Enough,” J. Grad. Med. Educ., **4**(3), pp. 279–82.

[73] Tong, J., Rezai, P., Salam, S., Selvaganapathy, P. R., and Gupta, B. P., 2013, “Microfluidic-based electrotaxis for on-demand quantitative analysis of Caenorhabditis elegans’ locomotion.,” J. Vis. Exp., (75), p. e50226.

[74] Yuan, J., Raizen, D. M., and Bau, H. H., 2015, “Propensity of undulatory swimmers, such as worms, to go against the flow,” Proc. Natl. Acad. Sci. U. S. A., **112**(12), pp. 3606–3611.

[75] Dasari, S., and Cooper, R. L., 2004, “Monitoring Heart Rate in Drosophila Larvae by Various Approaches,” Biol. Fac. Publ., p. Paper 69.

[76] Papoy, A. R., Ward, M., and Cooper, R. L., 2010, “Roles of the Sarcoplasmic / Endoplasmic Reticulum Ca 2 + -ATPase , Plasma Membrane Ca 2 + -ATPase and Na + / Ca 2 + Exchanger in Regulation of Heart Rate in Larval Drosophila,” Open Physiol. J., (3), pp. 16–36.

[77] Trappe, J. M., Molina, R., and Castellano, M., 1984, “Reactions of mycorrizal fungi and mycorrizal formation to pesticides,” Annu. Rev. Phytopaythology, **22**(22), pp. 331–359.

[78] Francis, D., Warren, S. A., Warner, K. J., Harris, W., Copass, M. K., and Bulger, E. M., 2010, “Sodium azide-associated laryngospasm after air bag deployment,” J. Emerg. Med., **39**(3).

[79] Sadiq, M. F., and Owais, W. M., 2000, “Mutagenicity of sodium azide and its metabolite azidoalanine in Drosophila melanogaster.,” Mutat. Res., **469**(2), pp. 253–7.

[80] González-César, E., and Ramos-Morales, P., 1997, “Sodium azide induces mitotic recombination in Drosophila melanogaster larvae,” Mutat. Res. - Genet. Toxicol.

Environ. Mutagen., **389**(2-3), pp. 157–165.

[81] Olajide, O. J., Enaibe, B. U., Bankole, O. O., Akinola, O. B., Laoye, B. J., and Ogundele, O. M., 2015, "Kolaviron was protective against sodium azide (NaN3) induced oxidative stress in the prefrontal cortex," Metab. Brain Dis., **31**, pp. 25–35.

[82] Delgado-Cortés, M. J. . b, Espinosa-Oliva, A. M. . b, Sarmiento, M. . b d, Argüelles, S. . b, Herrera, A. J. . b, Mauriño, R. . b, Villarán, R. F. . b, Venero, J. L. . b, Machado, A. . b, and De Pablos, R. M. . b c, 2015, "Synergistic deleterious effect of chronic stress and sodium azide in the mouse hippocampus," Chem. Res. Toxicol., **28**(4), pp. 651–661.

[83] Deshpande, R. G., and Khan, M. B., 1998, "Invasion of Aortic and Heart Endothelial Cells by Porphyromonas gingivalis Invasion of Aortic and Heart Endothelial Cells by Porphyromonas gingivalis," **66**(11), pp. 5337–5343.

[84] Guerenstein, P. G., Yepez, E. A., Van Haren, J., Williams, D. G., and Hildebrand, J. G., 2004, "Floral CO2 emission may indicate food abundance to nectar-feeding moths," Naturwissenschaften, **91**(7), pp. 329–333.

[85] Vermehren-Schmaedick, A., Ainsley, J. A., Johnson, W. A., Davies, S. A., and Morton, D. B., 2010, "Behavioral responses to hypoxia in drosophila larvae are mediated by atypical soluble guanylyl cyclases," Genetics, **186**(1), pp. 183–196.

[86] Morton, D. B., 2011, "Behavioral responses to hypoxia and hyperoxia in Drosophila larvae molecular and neuronal sensors," Fly (Austin)., **5**(2), pp. 119–125.

[87] Zarndt, R., Piloto, S., Powell, F. L., Haddad, G. G., Bodmer, R., and Ocorr, K., 2015, "Cardiac responses to hypoxia and reoxygenation in Drosophila.," Am. J. Physiol. Regul. Integr. Comp. Physiol., **309**(11), pp. 1347–1357.

[88] Scholey, A. B., Moss, M. C., Neave, N., and Wesnes, K., 1999, "Cognitive Performance, Hyperoxia, and Heart Rate Following Oxygen Administration in Healthy Young Adults," Physiol. Behav., **67**(5), pp. 783–789.

[89] Jamieson, D., Chance, B., and Cadenas, E., 1986, "Tthe relation of free radical production to hyperoxia," Ann. Rev. Physiol., **48**(24), pp. 703–19.

[90] Landis, G. N., Abdueva, D., Skvortsov, D., Yang, J., Rabin, B. E., Carrick, J., Tavaré, S., and Tower, J., 2004, "Similar gene expression patterns characterize aging and oxidative stress in Drosophila melanogaster.," Proc. Natl. Acad. Sci. U.

S. A., **101**(20), pp. 7663–8.

[91] Feala, J. D., Omens, J. H., Paternostro, G., and McCulloch, A. D., 2008, "Discovering regulators of the Drosophila cardiac hypoxia response using automated phenotyping technology," Ann. N. Y. Acad. Sci., **1123**, pp. 169–177.

[92] Chen, Q., and Haddad, G. G., 2004, "Role of trehalose phosphate synthase and trehalose during hypoxia: from flies to mammals.," J. Exp. Biol., **207**(Pt 18), pp. 3125–3129.

[93] Harrison, J., Frazier, M. R., Henry, J. R., Kaiser, A., Klok, C. J., and Rascon, B., 2006, "Responses of terrestrial insects to hypoxia or hyperoxia," Respir. Physiol. Neurobiol., **154**(1-2), pp. 4–17.

[94] Ocorr, K., Fink, M., Cammarato, A., Bernstein, S., and Bodmer, R., 2009, "Semi-automated Optical Heartbeat Analysis of small hearts.," J. Vis. Exp., (31), pp. 3–6.

[95] Vogler, G., and Ocorr, K., 2009, "Visualizing the beating heart in Drosophila.," J. Vis. Exp., (31), pp. 6–8.

[96] Stirman, J. J. N., Harker, B., Lu, H., and Crane, M. M. M., 2014, "Animal microsurgery using microfluidics," Curr. Opin. Biotechnol., **25**, pp. 24–29.